TITLE

Rescuing bacterial genome replication: essential functions to repair a double-strand break and restart DNA synthesis

AUTHORS

Charles Winterhalter[*], Stepan Fenyk, Heath Murray[**]

AFFILIATION

Centre for Bacterial Cell Biology, Biosciences Institute, Newcastle University, Newcastle Upon Tyne, NE2 4AX, UK

AUTHOR LIST FOOTNOTES

*Correspondence: Charles.winterhalter@newcastle.ac.uk

**Correspondence: Heath.murray@newcastle.ac.uk

HIGHLIGHTS

- Single-strand discontinuities inactivate the bacterial replisome
- Nicks on the leading or lagging strand template differentially affect fate of the helicase
- Double-strand breaks are repaired via homologous recombination and elicit the replication restart pathway
- Resection often generates a DNA strand with a 5′-end that must be processed to ensure productive helicase reloading

SUMMARY

Many antibiotics indirectly generate reactive oxygen species (ROS) that can damage bacterial genomes. Oxidised nucleobases become genotoxic when they are targeted for repair through excision, generating a single-strand discontinuity that can be converted to a double-strand break (DSB) by an oncoming replication fork. Because the genomic location of nucleobase oxidation is stochastic, investigating the fate of DNA replication machinery (replisome) at single-strand discontinuities has been limited. Here we have addressed this issue by expressing Cas9 nickases in *Bacillus subtilis* to create site specific single-strand discontinuities in a bacterial chromosome. We find that nicks in either leading or lagging strand arrest bacterial replication fork progression and generate a DSB that requires repair using homologous recombination to allow replication restart. These discoveries provoke reassessment of the fundamental mechanism of bacterial homologous recombination and provide insights to the development of alternative antimicrobials by identifying a specific pathway that can potentiate ROS-dependent bacterial killing.

KEYWORDS

DNA, replication, nick, helicase, fork, homologous repair, recombination, PriA, restart.

INTRODUCTION

Emergence of antibiotic resistant bacterial pathogens represents an urgent threat to human health and food production[1]. Understanding how bacteria respond to antibiotics is necessary to generate effective treatments. While antibiotics generally target specific essential bacterial systems (e.g. cell wall synthesis, translation, transcription) to inhibit bacterial proliferation, there is growing evidence that diverse antibiotics share the potential to disrupt bacterial physiology, thereby generating a second challenge to pathogens[2]. Work in several bacterial species indicates that a range of antibiotics ultimately generate reactive oxygen species (ROS) which can damage biomolecules including DNA[3,4]. Importantly, antibiotics that generate ROS elicit the bacterial DNA damage response, indicating the presence of double-strand breaks (DSB) under these conditions[4-7].

The potency of ROS-mediated DNA damage has been suggested to arise from conflicts between genome repair and replication systems[4-6,8]. Oxidised nucleobases located within the genome must be excised as part of the requisite repair pathway, leading to transient single-strand discontinuities in the DNA template[9]. If a bacterial replication fork arrives at a single-strand discontinuity, the encounter generates a DSB[10]. Elegant experiments using bacteriophage *λ* demonstrated that an engineered nick in either strand of the viral genome generated replication-dependent DSBs (Fig. 1A)[11]. While active DNA replication is necessary to generate DSBs at a nick, the fate of the bacterial DNA replication machinery (replisome) at single-strand discontinuities has not been determined.

The replisome is a multicomponent complex of proteins and enzymes that unwinds the chromosome and coordinates synthesis of new DNA polymers on the leading and lagging strands[12,13]. The most stable component of the replisome and most pivotal for its processivity is helicase[14,15]. Cellular replicative helicases are toroid enzymes that unwind DNA by encircling and translocating along a single client nucleic acid strand, acting as a wedge to disrupt base pairing[16]. Studies of bacterial replisomes *in vitro* and *in vivo* have revealed that the machinery is intrinsically dynamic, with most factors observed to bind and unbind interaction partners multiple times per replication cycle[17,18]. This behaviour enables

the replisome to overcome a range of potential roadblocks and remain associated with the template, competent to continue DNA synthesis[19]. However, recent studies in eukaryotic systems have indicated that single-strand discontinuities generate DSBs and arrest DNA replication by impairing helicase progression[20,21].

Determining how bacteria react and respond when a replication fork encounters a single-strand discontinuity is crucial to understanding how ROS inhibits bacterial proliferation. Here we have investigated this question by expressing Cas9 nickases (nCas9) in the model bacterium *Bacillus subtilis*. The results show that a nick located in either template strand blocks downstream DNA synthesis, and that resumption of DNA replication is dependent upon a core set of homologous recombination proteins and the PriA-dependent replication restart system necessary to reload the replicative helicase. Unexpectedly, interrogation of the DNA repair pathway suggests that processing of the DSB often leaves the 5′-terminated DNA strand intact, which can hybridise to the homologous chromosome during recombination and perturb replication restart. We ascribe the enigmatic RecG helicase as the factor that remodels these recombination products containing a 5′-terminated DNA strand, thereby generating the replication fork structure recognised by PriA for productive helicase loading. These findings have critical implications for the fundamental mechanism of homologous recombination in bacteria and the aim of potentiating ROS-dependent antibiotic toxicity.

RESULTS

Single-strand discontinuities in a bacterial chromosome arrest DNA synthesis

Oxidised nucleobases generated by ROS can be located randomly throughout a genome, making it a challenge to directly analyse conflicts with DNA replication during base excision repair. To mimic the activity of oxidised base repair, an experimental system capable of generating a site-specific single-strand discontinuity was developed in *B. subtilis* using Cas9 nuclease variants and single-guide RNAs (sgRNA)[20-23]. Cas9 carrying single amino acid substitutions ($Cas9^{D10A}$ or $Cas9^{H840A}$) created nickases (nCas9), while the double mutant ($Cas9^{D10A/H840A}$) created a catalytically inactive enzyme (dCas9)[24]. Each *cas9* allele was integrated into the *B. subtilis* chromosome under the control of a xylose-inducible promoter (Fig. 1B)[25]. The location of sgRNA hybridisation is indicated by coordinates between the origin (0°) and terminus (~180°) on either the right (+) or left (-) replicore of the chromosome. To avoid complications arising from potential activation of prophage following DNA damage in the laboratory strain of *B. subtilis*, a derivative lacking these genetic elements (Δ6) was used throughout this study[26].

Cell viability was quantified using spot-titre assays, where strains are grown to saturation in liquid medium without xylose, before samples were serially diluted and plated onto solid medium with or without xylose to enumerate the number of colony forming units (CFUs). It was observed that the $Cas9^{D10A}$ nickase elicited a stronger phenotype than $Cas9^{H840A}$ upon induction with xylose (Fig. S1A-B)[24]. To achieve comparable nicking efficiency at different sites in the chromosome, the *cas9*^{D10A} allele was used throughout the remainder of this study, in conjunction with distinct sgRNAs targeted to the template of either the leading or the lagging strand (in non-essential regions of the genome). Using sgRNAs to target leading and lagging strands at loci on both left and right chromosome arms, it was observed that expression of nCas9 resulted in severe growth inhibition (Figs. 1C, S1C). In contrast, expression of dCas9 targeted to the same locations did not affect the number of CFUs (Figs. 1C, S1D), indicating that DNA nicking was necessary for the observed growth defect.

Next chromosome replication was investigated using whole genome marker frequency analysis (MFA). Expression of Cas9 variants was induced for one hour in exponentially growing cultures. Genomic DNA (gDNA) was harvested for next-generation sequencing, reads were mapped onto the reference genome sequence, and data is displayed with the chromosome origin (*oriC*) at the center of the graphs (Fig. S2). It was observed that nicks in either the leading or lagging strand resulted in a drop in sequencing coverage from the nick site to the terminus region, whereas expression of dCas9 with the same sgRNAs did not appear to inhibit DNA replication (Fig. 1D). Because cells expressing nCas9 are unable to synthetise DNA downstream of the nick, this likely explains the strong growth inhibition observed in spot-titre assays (Fig. 1C).

Previous results indicated that a replication fork encountering a single-strand discontinuity generates a DSB[11]. To determine whether DSBs were being formed in *B. subtilis* following nCas9 induction, localisation of the reporter mNeonGreen-RecA (mNG-RecA) was observed in live cells using fluorescence microscopy. It has been shown that following artificial endonuclease cleavage to create a DSB, fluorescently labelled RecA recombinase assembles into bundles[27-29]. Prior to induction of nCas9, mNG-RecA is observed evenly distributed over the nucleoid (Fig. S3A). Following expression of nCas9 for one hour during exponential growth, mNG-RecA bundles were detected in 58.5% of cells when the leading strand template was nicked and 48% of cells when the lagging strand template was nicked (Figs. 1E-F, S3B). In contrast, expression of dCas9 did not significantly promote mNG-RecA bundling (Figs. 1E-F, S3B). These results are consistent with the model that collision of a replication fork with a nick in either strand of the parental DNA duplex generates a DSB.

Single-strand discontinuities in a bacterial chromosome inactivate the replisome

MFA indicated that under conditions expressing nCas9, DNA synthesis does not proceed beyond the nick. We wondered whether the replisome becomes arrested at a single-strand discontinuity, or rather whether the replication fork collapses. If the latter event occurs, then

the bacterial replication restart system would be required to reload helicase and promote replisome assembly[30,31]. In *B. subtilis* there is only one known restart system composed of the essential proteins PriA and the helicase loaders DnaD, DnaB, and DnaI (note that in *B. subtilis* the replicative helicase is DnaC)[32-36].

Chromatin immunoprecipitation (ChIP) followed by quantitative PCR (qPCR) was used to determine the enrichment of helicase and replication restart proteins surrounding a nick in either the leading or lagging strand template. Following induction of nCas9 for one hour in exponentially growing cells, samples were harvested for ChIP. Along with sites flanking the nick region, protein enrichment was also probed at the origin *oriC* as positive control and normalised to a site located on the opposite chromosome arm equidistant from *oriC* (+90, Fig. 2A). ChIP showed that helicase is specifically enriched upstream of nicks located in either template strand (Figs. 2B, S4). This upstream helicase enrichment was not detected when dCas9 was expressed, indicating that the Cas9-sgRNA nucleoprotein complex alone does not stall replication fork progression (Figs. 2B, S4).

Interestingly, significant enrichment of helicase was observed downstream of the nick site only when cleavage occurred in the template used for leading strand synthesis (Figs. 2B, S4). Because the bacterial replicative helicase translocates along a single strand in the 5′→3′ direction, ChIP results suggest that when the template for the lagging strand is nicked helicase runs-off the DNA substrate, whereas when the template for the leading strand is nicked helicase progresses downstream of the single-strand discontinuity (Fig. 2G). Consistent with the ChIP enrichment observed *in vivo* (Fig. 2A-B) and replisome inactivation (Fig. 1D), reconstituted unwinding assays *in vitro* using bacterial helicase on model replication fork substrates have shown that if a flap is absent from the substrate (i.e. mimicking a nick), helicase transitions from encircling a single DNA strand onto double-stranded DNA (dsDNA) and slides along the duplex, no longer able to unwind[37].

The enrichment of helicase upstream of nick sites is consistent with either helicase stalling or helicase reloading via the replication restart pathway. To distinguish between these models, ChIP was used to probe for the presence of replication restart proteins

surrounding the nicks. Following nCas9 induction, enrichment of PriA, DnaD, DnaB and DnaI was detected upstream (but not downstream) of the sgRNA target sequences, while these proteins were absent from this region when dCas9 was expressed (Fig. 2C-F). These results suggest that nicks in either the leading or lagging strand template elicit the replication restart pathway for helicase reloading, whether helicase falls off the template (lagging strand template nick) or translocates downstream (leading strand template nick) in an inactive state (Fig. 2G).

A weakened nCas9 system permits DNA replication restart

While replication restart proteins were enriched upstream of nick sites (Fig. 2B-F), viability assays and MFA both indicated that downstream DNA synthesis was inhibited (Fig. 1C-D). We speculated that persistent nCas9 cleavage activity competes with productive DNA replication restart. Therefore, to allow interrogation of processes occurring downstream of DNA cleavage and replisome collapse, a weaker nCas9 system was developed. An *ssrA* degradation tag[38] was fused to *cas9*^{D10A} to promote nCas9 proteolysis, and expression of both *nCas9-ssrA* and *sgRNAs* were placed under the control of xylose-inducible promoters (Fig. S5A). In this background, induction of nCas9 did not significantly inhibit cell viability or chromosome content (Fig. S5B-C) and MFA showed that DNA synthesis continued after a one-hour xylose induction, consistent with low tolerable levels of nickase activity (Fig. 2H). This weakened nicking system was employed for all experiments described below.

PriA is required to restart DNA replication at single-strand DNA discontinuities

The master replication restart factor *priA* is essential for growth of *B. subtilis.* To ascertain whether PriA-dependent replication restart is required following chromosome nicking, a titratable PriA complementation system was developed (Fig. S6A). Here conditions were established to express PriA-ssrA at a low level, sufficient to maintain *B. subtilis* viability while limiting the amount of PriA activity within a cell (Fig. S6B-C). When nCas9-ssrA and sgRNA were induced with limiting PriA-ssrA, spot-titre analyses showed that cell growth was

inhibited in the absence of the endogenous *priA* copy (Fig. 2I-J). Yet in this background, higher expression of PriA-ssrA rescued viability (Fig. S6D). Following induction of nCas9 and sgRNA for one hour during exponential growth, MFA showed that limited levels of PriA-ssrA could not sustain chromosome synthesis downstream of the nick site (Fig. 2K). Therefore, these data indicate that PriA is essential to restart DNA replication following replisome inactivation at single-strand DNA discontinuities.

The DSB resulting from a single-strand discontinuity is repaired using a core set of homologous recombination proteins

Cytological analysis indicated that a nick in the template of either the leading or lagging strand generated a DSB (Fig. 1E). Strong evidence indicates that in bacteria such DSBs are repaired by homologous recombination, thereby recreating a replication fork to allow resumption of DNA synthesis[39]. To determine the factors required to repair DSBs following nCas9 nicking, a targeted reverse genetic analysis was employed, focused on genes previously implicated in homologous recombination and other DNA repair processes (Table S1). Using this approach, spot-titre analyses revealed that eight non-essential genes were required for normal growth upon nick induction: DNA end-processing genes *addA*/*addB* and homologous recombination genes *recF*/*recO*/*recR*/*recA*/*recG*/*recU* (Fig. 3A and S7A). Functional complementation of each synthetic lethal deletion confirmed that these gene products are necessary to support growth in cells expressing nCas9 (Fig. S7B). Surprisingly, the screen revealed that several factors implicated in DNA repair are not essential under these conditions, such as those classed for end-processing (RecQ, RecS, RecJ)[7,40], maintaining chromosome structure ("SMC-like" RecN, SbcCD, SbcEF)[41,42], recombination mediation (RecD2, RecX)[43-45] and Holliday junction migration (RuvA, RuvB)[40] (Fig. S8).

Focusing on the eight mutants that produced a clear growth defect, MFA was used to analyse DNA replication following induction of nCas9 and sgRNA in exponentially growing cells. The results showed that DNA end-processing (*addA*/*addB*) and recombination mutants (*recF*/*recO*/*recR*/*recA*/*recG*) are defective in chromosome replication downstream of the nick

site, with the only exception being *recU* (Fig. 3B; note subtle differences in replication profiles of parental strains containing deletions of homologous recombination genes, consistent with previous findings[46,47]). These observations support the hypothesis that homologous recombination is necessary to repair the DSB and restart DNA replication.

Based on the proposed activities of these proteins, the following model was developed (Fig. 3C). AddAB helicase/nuclease processes the DSB to generate a single-stranded substrate with a 3′-end required for recombination[48,49]; RecFOR displaces the single-stranded binding protein (SSB) from single-stranded DNA substrates produced by AddAB, thereby allowing RecA to bind[50,51]; RecA is the recombinase that binds to single-stranded DNA (ssDNA) with a free 3′-end, identifies homologous DNA on the non-broken chromosome, and performs strand invasion and exchange[52,53]; RecU resolves the Holliday junction generated by RecA[54]. The role of RecG *in vivo* is enigmatic[55,56] and discussed further below.

The SSB C-terminal tail is required for DNA repair following replisome inactivation

The requirement of the RecFOR system for repair of a seDSB strongly suggested that the essential single-strand binding protein (SSB) was also involved. To interrogate this hypothesis, recruitment of SSB was probed using ChIP following induction of nCas9 and sgRNA in exponentially growing cells. The results showed that SSB is enriched upstream of either leading or lagging strand nicks (Fig. 4A). SSB enrichment ~3 kb upstream from the nick site was dependent upon AddAB but independent of the remaining factors required for homologous recombination (Fig. 4B), indicating that AddAB is necessary to generate ssDNA for SSB.

SSB forms a homotetramer that binds ssDNA non-specifically via its N-terminal domain. Each SSB monomer harbours a long disordered C-terminal domain that contains a protein interaction sequence at the terminus (the C-terminal tail or CTT) (Fig. S9A-B)[57]. While the *B. subtilis* SSB-CTT is dispensable for cell viability, it is required for efficient repair of DNA lesions created by either UV irradiation or Mitomycin C treatment [42,58].

To determine whether the SSB-CTT is required for repair of a DSB following replisome inactivation at a nick, an IPTG-inducible SSB complementation system was generated in a Δ*ssbA* strain, allowing expression of either the wild-type protein or a variant lacking the last six amino acids ($SSB^{\Delta CTT}$, Fig. S9C). Spot-titre analyses confirmed that $SSB^{\Delta CTT}$ can complement a Δ*ssbA* mutant similar to wild-type SSB and that viability was dependent upon IPTG (Fig. S9D), and immunoblots showed that the inducible SSB proteins were being expressed at levels comparable to the endogenous protein (Fig. S9E).

The SSB complementation system was then moved into strains expressing nCas9 and sgRNA (Fig. S9F). Spot titre analyses showed that wild-type SSB was able to support viability following induction of nCas9 and sgRNA, whereas the $SSB^{\Delta CTT}$ variant could not (Fig. 4C). MFA confirmed that chromosome replication from the nick site to the terminus is arrested when SSB lacks its C-terminal tail (Fig. 4D). Therefore, the results indicate that the SSB-CTT is necessary for DNA repair following replisome inactivation at a nick.

The SSB-CTT is required to recruit RecO to the site of DNA repair during homologous recombination

The SSB-CTT acts as a protein interaction hub[42] that directly interacts with several factors found to be necessary for repair of a DSB, including RecO, RecG, and PriA (Figs. S9G, 2I-K, 3A-B). To investigate the essential role of the SSB-CTT, ChIP was employed to probe the recruitment of SSB variants, His-RecO, and His-RecA upstream of nick sites. ChIP showed that the $SSB^{\Delta CTT}$ variant remained enriched upstream of nicks at similar levels to the wild-type protein (Fig. 4E). However, enrichment in His-RecO and His-RecA was lost in cells harbouring $SSB^{\Delta CTT}$ (Fig. 4E), indicating that the SSB:RecO interaction depends on the SSB-CTT (Fig. S9H). In cells encoding wild-type SSB, enrichment of His-RecA was dependent upon both AddAB and RecFOR (Fig. 4F), consistent with the model that RecFOR is necessary for RecA loading onto ssDNA substrates bound by SSB. Taken together, these

results indicate that an essential role of the SSB-CTT is to recruit RecO to repair sites following replisome inactivation at single-strand DNA discontinuities.

What is the essential role of RecG for restart of DNA replication?

While the role of most factors required for resuming DNA replication following replisome inactivation at a single-strand discontinuity could be rationalised, the role of RecG was unclear. RecG has been implicated in a myriad of DNA transactions including reversal of replication forks, migration of Holliday junctions, regulation of RecA strand exchange, processing of flaps generated when DNA replication forks converge, and stabilisation of D-loops[56,59-62].

Examination of the MFA in a Δ*recG* mutant showed that there was an increase in sequence read depth upstream of a nick targeted to either the leading or lagging strand template (Fig. 5A), suggesting that DNA synthesis increases in this region in the absence of RecG. This observation was reminiscent of results reported in *Escherichia coli* during DSB repair in a Δ*recG* mutant, where it was proposed that RecG remodels intermediate DNA structures formed during homologous recombination to ensure PriA is correctly orientated to load helicase (Fig. 5B, in the absence of RecG helicase reloading occurs on the opposite strand normally used for DNA replication, thus directing inappropriate DNA synthesis from the terminus towards *oriC*)[47]. This hypothesis diverges from the generally accepted model for homologous recombination, in which resection of a DSB involves degradation of the strand with a 5′-end, thereby generating a single-stranded 3′-end substrate for recombinases (e.g. RecA, Fig. S10). The revised model instead suggests that following DNA end-processing, the strand containing a 5′-end remains intact and can hybridise the displaced strand (D-loop) formed as a consequence of RecA strand invasion[47]. It was suggested that this intermediate DNA structure was the substrate for RecG, such that the enzyme would remodel the strands by unwinding the annealed 5′-end until the annealed 3′-end abutted the fork junction, thus generating the correct substrate for PriA to reload helicase (Fig. S11)[63]. Biochemical data using purified proteins has shown that RecG and PriA can perform these

activities on model replication fork substrates[63,64]. Therefore, we sought to test this hypothesis *in vivo* using the nCas9 system.

RecG is required to remodel replication forks formed when a DSB contains a 5′-end

The genetic analysis above indicated that the AddAB helicase/nuclease was responsible of end processing of the DSB (Fig. 3A). While both AddA and AddB subunits harbour nuclease activity, the two enzymes cleave distinct strands of the DNA duplex following unwinding by AddA helicase activity (AddA cleaves the strand terminating with a 3′-end, AddB cleaves the strand terminating with a 5′-end)[49]. Therefore, it was hypothesised that inactivating either AddA or AddB nuclease activity would bias DSB processing to favour the generation of either a 3′-tail (AddA nuclease mutant) or a 5′-tail (AddB nuclease mutant).

To begin, ChIP was used to confirm that AddAB was acting directly on the DSB generated following replisome inactivation at a nick. AddA and AddB were independently fused to the fluorescent protein *mNeonGreen* and enrichment of each subunit was determined. The results showed that mNG-AddA and mNG-AddB are both enriched upstream of nicks, consistent with their direct role in end-processing under these conditions (Fig. 5C).

Next, the enzymatic activities of AddA and AddB were reduced through substitution of catalytic residues[49]. Spot titre analyses showed that the helicase defective $AddA^{K36A}$ ($AddA^{\Delta HEL}$) was unable to sustain bacterial growth upon induction of nicks, whereas nuclease defective variants of either $AddA^{D1172A}$ ($AddA^{\Delta NUC}$) or $AddB^{D961A}$ ($AddB^{\Delta NUC}$) grew similar to a strain with wild-type AddAB (Figs. 5D, S12A). Notably, the double nuclease variant $AddA^{\Delta NUC}AddB^{\Delta NUC}$ also supported normal growth (Fig. 5D), suggesting that under these conditions in live cells the DSB may not require resection. MFA confirmed that DNA synthesis was blocked downstream of a nick in the strain expressing $AddA^{\Delta HEL}$, while the strains expressing $AddA^{\Delta NUC}$, $AddB^{\Delta NUC}$ or $AddA^{\Delta NUC}AddB^{\Delta NUC}$ were comparable to wild-type (Figs. 5E, S12B-C). Moreover, ChIP demonstrated that SSB is not enriched upstream of nicks in a strain expressing $AddA^{\Delta HEL}$, whereas SSB was enriched in $AddA^{\Delta NUC}$ and

AddB$^{\Delta NUC}$ backgrounds (Fig. 5F). Together these results indicate that AddAB helicase activity is directly required to process a DSB generated after replisome inactivation at a nick, and that nuclease activity can be abolished without compromising DNA replication restart.

Finally, the Δ*recG* mutant was moved into strains expressing either AddA$^{\Delta NUC}$ or AddB$^{\Delta NUC}$ and nicking was induced (Fig. 6A-B). Spot-titre assays showed that RecG remained essential in the strains containing AddB$^{\Delta NUC}$, where degradation of the strand terminating with a 5′-end is inhibited (Fig. 6C). Strikingly, in the AddA$^{\Delta NUC}$ strain where degradation of the strand terminating with a 3′-end is inhibited, the absence of RecG was well tolerated (Fig. 6C-D). These results are consistent with the model that RecG is required to remodel recombination intermediates that contain a single-strand with a 5′-end annealed to a D-loop. Importantly, the critical role of RecG in strains with single-strand discontinuities (Fig. 3A) implies that wild-type processing of a DSB often generates a single-strand with a 5′-end, which is inconsistent with most current models of bacterial homologous recombination.

DISCUSSION

In this study we have characterised the fate of the bacterial replisome *in vivo* after it encounters a single-strand discontinuity in the DNA template (Fig. 1A). The results indicate that a nick in the template for either the leading or lagging strand arrests DNA synthesis, generates a DSB, and elicits replication restart following repair of the DNA break through homologous recombination (Figs. 1-3). These findings are consistent with the observation that a nick in a replicating bacteriophage chromosome generates DSBs[11] and with recent reports of the impact of nicks in eukaryotic replication systems[20,21,23]. Importantly, while replisomes are thought to be generally intolerant to many types of DNA damage[65], it appears that the bacterial replication machinery cannot readily bypass single-strand interruptions as these lesions affect helicase progression (Figs. 2, 7(I)).

Repair of the DSB to facilitate replication restart requires homologous recombination (Fig. 3). Genetic analysis combined with ChIP indicates that a single pathway is utilised under these experimental conditions (Fig. 7): AddAB unwinds the DNA; SSB binds the ssDNA; RecFOR counteracts SSB and allows RecA to bind ssDNA; RecA promotes strand invasion of the homologous chromosome and generates a D-loop, which often anneals to a single-strand with a 5′-end; RecG regresses the fork and simultaneously separates the annealed strand with a 5′-end; PriA binds to the remodelled fork where it interacts with the strand harbouring a 3′-end and reloads helicase to promote replisome assembly and DNA replication restart. The observed lack of redundancy between proteins involved in recombinational DNA repair suggests that the pathway identified here is the major route for fixing this type of collapsed replication fork in *B. subtilis*[41,66].

Building upon these results, we investigated specific protein activities to help elucidate their roles during recombinational repair of a DSB. Below we discuss these findings in what we propose is chronological order.

The replicative helicase is inactivated after it encounters a nick

In bacteria the replicative helicase encircles and tracks along the template for lagging strand synthesis. ChIP data suggests that there are distinct fates of the helicase depending on the location of a nick (Figs. 2A-B, S4). As expected for a nick in the lagging strand template, helicase enrichment was only observed at the cleavage site and upstream, consistent with the model that helicase runs-off the template when it encounters the single-strand discontinuity (Figs. 2G, 7(I)). In contrast, when the nick was in the leading strand template, helicase was also enriched downstream of the cleavage site, suggesting that the enzyme continued translocation. We propose that upon encountering a nick in the leading strand template, helicase slides onto the dsDNA template in an inactive conformation that cannot perform further DNA unwinding (Figs. 2G, 7(I)). This model is consistent with *in vitro* experiments using *Thermus aquaticus* helicase, where after unwinding up to a nick on the leading strand template, the enzyme can continue to translocate with the two strands of DNA passing through the central channel with no resultant unwinding[37]. Whether the bacterial helicase is actively removed from dsDNA under these conditions, akin to what has been observed for the eukayotic CMG helicase in *Xenopus* extracts[20], requires further investigation.

AddAB helicase activity is necessary and sufficient for recombinational repair

AddAB and related enzymes have been shown to bind blunt end dsDNA or dsDNA with short overhangs (4-20 nucleotides with either a 5′- or a 3′-end)[49,67]. When the template for leading strand synthesis is nicked, the DNA polymerase likely runs-off the end of the substrate to produce a blunt or nearly blunt end, suitable for recognition by AddAB. However, when the template for lagging strand synthesis is nicked, a substrate with a 3′-tail would likely be produced. Because the reverse genetic screen suggested that no additional nucleases are required for this recombinational repair pathway (Figs. 3, S8), we speculate that the high local concentration of replication factors would facilitate priming near the end of the 3′-tail, thereby filling the ssDNA with an Okazaki fragment to create a suitable substrate for AddAB.

The master recombination factor RecA requires ssDNA to promote homologous pairing. A long-standing question is how this ssDNA is generated *in vivo*. Most current models suggest that enzymes resect a DSB to generate a single-strand terminating with a 3′-end[7,31]. Here we tested this model by mutating the nuclease activities of AddA and AddB. The results showed that neither nuclease activity is required for enzyme function under the experimental conditions tested (Figs. 5D-E, S12B-C). In contrast, AddAB helicase activity was required for recombinational repair, consistent with a previous study of the ancestral AdnAB resection machinery in *Mycobacteria tuberculosis*[68]. These results suggest that the key role of AddAB is not to digest the dsDNA ends, but rather to separate the strands and create the ssDNA substrate for SSB (Figs. 5F, 7(II-III)).

The local concentration of SSB is high at the site of DNA replication[69,70], potentially facilitating its rapid association with the ssDNA emerging from AddAB. In fact, *in vitro* the $AddA^{NUC}AddB^{NUC}$ nuclease-dead enzyme does not unwind dsDNA in the absence of SSB[71], suggesting that AddAB unwinding and SSB binding ssDNA may be coupled. We propose that AddAB nuclease activity represents a secondary method of generating a ssDNA substrate for SSB, following initial AddAB helicase activity required to separate the DNA duplex.

Interaction of the SSB C-terminal tail with RecO is necessary for replication repair

The SSB-CTT is an established protein interaction hub that has been shown to directly bind several of the essential replication and repair factors required at nicks, including RecO[72-75], RecG[76,77], and PriA[58,78]. However, the critical activities performed by the SSB-CTT *in vivo* have not yet been established[42]. Based on the results above, we conclude that the SSB-CTT interaction with RecO is necessary for replication repair. RecO is part of the RecFOR system required for RecA loading onto ssDNA *in vitro*[79] and RecA-GFP foci formation *in vivo*[80]. Because RecO activity occurs before the activities of RecG and PriA (i.e. RecA binding ssDNA is blocked, Fig. 4F), this precludes further conclusions regarding the importance of these protein:protein interactions at this time.

In vitro the RecO:RecR complex facilitates loading of RecA onto SSB-coated ssDNA[81,82]. Because RecO, RecR, and RecF were all required for replication repair, we propose that the essential role of RecF here is to recruit RecR and generate the RecO:RecR complex. This model is consistent with a hand-off mechanism for RecR observed *in vitro*[81]. RecF is a dimeric ATPase that adopts a clamp conformation around dsDNA[51]. Recent studies in *E. coli* have shown that recruitment of RecF to sites of repair is mediated by the DNA polymerase sliding clamp processivity factor DnaN[82]. As was the case for SSB[70], the local concentration of DnaN is high near the sites of DNA replication collapse[69], thereby potentially facilitating RecF recruitment. Importantly for this model, since both SSB and DnaN are enriched at a replication fork, we predict that there is a mechanism to regulate RecO:RecR complex formation until it is required, thus safeguarding the SSB-coated strand from promiscuous RecA loading (Figs. 4B, 4F, 7(III-V)).

RecG remodels a repaired replication fork by unwinding dsDNA with an exposed 5′-end

The biological role of RecG has been a long-standing question[55,56]. *In vitro* RecG is a DNA translocase that unwinds a myriad of DNA substrates, including Holliday junctions, D-loops, and model replication forks[47,60-62,64]. Here MFA indicates that a *ΔrecG* mutant cannot efficiently restart DNA replication at a nick directed to either the leading or the lagging strand template (Figs. 3B, 5A-B), consistent with a role in fork remodelling[46]. Based on genetic experiments and supported by biochemical assays *in vitro*, a model has been presented for RecG binding to a replication fork and unwinding dsDNA on the lagging strand template to allow correct orientation of PriA for helicase loading[47,63]. Critically, this model requires that the single strand with a 5′-end from the DSB can hybridise with ssDNA of the D-loop on the homologous chromosome.

How this predicted intermediate structure is constructed remains to be determined, but the implication is that the separated strands of the DSB are either the same length or the strand with a 5′-end is longer (Figs. 6A, 6D, 7(VI-VII)). This model contrasts with most

current views of bacterial DSB end-processing where a single strand with a 3′-end is produced for RecA (Fig. S10)[7,31,83]. Moreover, because RecG is essential in strains expressing Cas9 nickases, it suggests that during wild-type DSB end-processing the separated strands often contain a 5′-end that requires remodelling by RecG (Fig. 7(VII)). These unanticipated results, together with those of the accompanying manuscript analysing resolution of collapsed eukaryotic replication forks[84], necessitate further evaluation of DSB management following replisome collapse across all domains of life.

Holliday junction migration and resolution are not necessary for replication restart

Branch migration of a Holliday junction is generally considered a hallmark of homologous recombination, therefore it was notable that the canonical Holliday junction translocase RuvAB was not required for replication repair at nicks (Fig. S8D). In fact, the *ΔrecU ΔruvAB* knockout attenuated the penetrance of the *ΔrecU* mutant upon introduction of single-strand discontinuities, suggesting that either another enzyme can functionally complement RuvAB activities or that branch migration is not required for this repair pathway.

While genetic analysis shows that RecU is required for wild-type growth following expression of Cas9 nickases, MFA indicates that RecU is not necessary for replication restart *per se* (Fig. 3). These results are consistent with the model that RecU resolves the Holliday junction formed during recombinational repair[85]. We hypothesise that the growth defect observed in the *ΔrecU* mutant may be caused by aberrant chromosome segregation[85], as the recombined DNA molecules need to be separated prior to completing cell division. It is known that multiple systems can facilitate chromosome separation following replication (e.g. Topoisomerase IV, XerD)[86,87], potentially explaining why the growth defect of the *ΔrecU* mutant under these experimental conditions was less severe compared to the other recombination mutants identified.

Potentiating ROS-mediated antibiotic toxicity by perturbing DNA repair

In this work, the nicks generated by Cas9 enzymes were used as proxies for single-strand discontinuities formed during removal of damaged DNA from a bacterial genome. We find that when a bacterial replication fork encounters a single strand discontinuity it becomes inactivated, likely contributing to the toxic effect of ROS-dependent damage induced by antimicrobials. By identifying the essential factors and activities required to repair the DSB formed after a replisome encounters a nick, we have provided a set of molecular targets whose disruption could potentiate the activity of antibiotics that produce ROS-dependent DNA damage.

RESOURCE AVAILABILITY

Lead contact

For additional information and requests for resources and reagents, please contact the lead contact: Charles Winterhalter (charles.winterhalter@newcastle.ac.uk).

Materials availability

Genetic materials generated in this study can be obtained directly from the lead contact.

Data and code availability

R code (DOI: 10.5281/zenodo.14793122) and protein structures for SSB:ssDNA and SSB:RecO complexes (DOI: 10.5281/zenodo.14793919) are available from Zenodo.

ACKNOWLEDGEMENTS

This work was supported by a Wellcome Trust Early-Career Award [226338/Z/22/Z] to CW and Wellcome Trust Discovery Award [225811/Z/22/Z] to HM. We would also like to express our gratitude to Frances Davison for technical assistance, James Grimshaw for microscope maintenance and Frederic Schramm for insightful discussions prior to submission.

AUTHOR CONTRIBUTIONS

CW and HM contributed to the conception/design of the work. CW and SF generated results presented in the manuscript. CW created figures. CW and HM wrote/edited the manuscript.

DECLARATION OF INTERESTS

The authors declare no competing interests.

DECLARATION OF GENERATIVE AI AND AI-ASSISTED TECHNOLOGIES

During the preparation of this work, the authors used AlphaFold 3 to generate SSB:ssDNA and SSB:RecO protein models. After using this tool, the authors reviewed the models and edited their content as needed and take full responsibility for the content of the publication.

STAR Methods

Key resources table

REAGENT or RESOURCE	SOURCE	IDENTIFIER
Antibodies		
Anti-Cas9 monoclonal	Merck	SAB4200701
Anti-FtsZ polyclonal	Eurogentec	Lucet *et al.* (2000)[88]
Anti-PriA polyclonal	Eurogentec	This study
Anti-SSB polyclonal	Eurogentec	This study
Anti-mNeonGreen monoclonal	ProteinTech	32F6
HRP-conjugated Goat Anti-Rabbit IgG (H+L)	ProteinTech	SA00001-2
HRP-conjugated Donkey Anti-Sheep IgG (whole molecule)	Merck	A3415
HRP-conjugated Goat Anti-Mouse IgG, Fcγ Fragment Specific	ProteinTech	SA00001-1-A
Anti-DnaD polyclonal	Eurogentec	Winterhalter *et al.* (2022)[33]
Anti-DnaB polyclonal	Eurogentec	This study
Anti-DnaI polyclonal	Eurogentec	This study
Anti-DnaC polyclonal	Eurogentec	This study
Anti-His monoclonal	Qiagen	34660
Bacterial strains		
See Table S2		
Chemicals		
Oxoid™ Nutrient agar	Thermo Scientific	CM0003B
Oxoid™ Tryptone	Thermo Scientific	LP0042B
Sodium chloride (NaCl)	VWR	27810.364P
Oxoid™ Yeast Extract Powder	Thermo Scientific	LP0021B
Ampicillin sodium salt	Merck	A9518
Erythromycin	Merck	E5389
Lincomycin hydrochloride	Merck	L6004
Chloramphenicol	Merck	C0378
Kanamycin disulfate salt	Merck	K1876
Spectinomycin dihydrochloride pentahydrate	Melford	S23000
Zeocin™ Selection Reagent	Invitrogen	R25001
D-(+)-Xylose	Merck	W360600
Isopropyl-β-D-thio-galactopyranoside (IPTG)	Melford	I56000
Ribonuclease A	Merck	R6513

Lysozyme	Merck	L6876
Ammonium sulphate	VWR	21333.296
di-Potassium hydrogen phosphate	VWR	26930.293
Potassium dihydrogen phosphate	VWR	26936.293P
tri-Sodium citrate dihydrate	VWR	27833.294P
Magnesium sulphate heptahydrate ($MgSO_4$)	VWR	25165.260
Ammonium iron(III) citrate	Merck	F5879
D-(+)-Glucose	VWR	101176K
L-Tryptophan	Formedium	DOC0189
Casein Peptone	Merck	22090
Ethanol	Fisher Scientific	12478740
Oxoid™ Phosphate Buffered Saline Tablets	Thermo Scientific	BR0014G
cOmplete™, Mini, EDTA-free Protease Inhibitor Cocktail	Roche	4693159001
DL-Dithiothreitol (DTT)	Melford	D11000
Methanol	Fisher Scientific	M/4000/17
TRIS base	Melford	T60040
Glycine	Merck	G7126
Tricine	Thermo Scientific	J64437.36
Sodium dodecyl sulfate (SDS)	Merck	75746
Ethylenediaminetetraacetic acid (EDTA)	Merck	03609
TWEEN® 20	Merck	P7949
Dried skimmed milk	Tesco	267377676
Calcium chloride dihydrate ($CaCl_2$)	Merck	C3306
Manganese(II) Sulfate Tetrahydrate ($MnSO_4$)	Fisher Scientific	M/2300/50
L-Glutamic acid potassium salt monohydrate	Merck	G1501
Sodium azide	Merck	S8032
Water, DEPC-Treated, DNASE/RNASE free, Fisher BioReagents™	Fisher Scientific	BP561-1
Formaldehyde solution	Merck	252549
Sucrose	Merck	S0389
Triton™ X-100	Merck	T8787
Protease from *Streptomyces griseus* (pronase)	Merck	P5147
Lithium chloride (LiCl)	Merck	L9650
IGEPAL® CA-630	Merck	I8896
Sodium deoxycholate monohydrate	Merck	D5670
Recombinant Proteinase K Solution	Invitrogen	AM2548
Commercial kits and equipment		

Q5® High-Fidelity DNA Polymerase	NEB	M0491L
KOD Xtreme™ Hot Start DNA Polymerase	Merck	71975
QIAprep Spin Miniprep Kit	Qiagen	27106
NEBuilder® HiFi DNA Assembly Cloning Kit	NEB	E5520S
QIAquick PCR Purification Kit	Qiagen	28106
DNeasy Blood and Tissue Kit	Qiagen	69504
Ultrasonic processors, Vibra-Cell™	Jencons-PLS	VC130
NuPAGE™ Bis-Tris Midi Protein Gels, 4 to 12%, 1.0 mm	Invitrogen	WG1402BX10
NuPAGE™ MES SDS Running Buffer (20X)	Invitrogen	NP0002
NuPAGE™ LDS Sample Buffer (4X)	Invitrogen	NP0007
Amersham™ Hybond® P membrane, PVDF	Merck	GE10600023
Wypall X60 cloths	Camlab	1206641
Trans-Blot Turbo Transfer System	Bio-rad	1704150
Clarity Western ECL Substrate	Bio-rad	1705061
ImageQuant™ LAS 4000 mini	GE Healthcare	28-9607-61 AB
DNA Prep IPB and buffers	Illumina	20049005
DNA Prep PCR and buffers	Illumina	20015826
DNA Prep CD indexes	Illumina	20015882
Qubit™ 1X dsDNA High Sensitivity (HS) kit	Invitrogen	Q33231
Qubit™ 4 Fluorometer	Invitrogen	Q33238
iSeq 100 i1 Reagent v2 sequencing chips	Illumina	20009555
iSeq 100 i1 Reagent v2 cartridges	Illumina	20009584
iSeq 100 Sequencing System	Illumina	20021532
GFP filter (EX470/40 DM495lpxr, EM525/50)	Chroma	49002
DAPI filter (EX350/50, DM400lp, EM460/50)	Chroma	49000
mCherry filter (EX560/40, DM585lprx, EM630/75)	Chroma	49008
Dynabeads™ Protein G for Immunoprecipitation	Invitrogen	10009D
Luna® Universal qPCR Master Mix	NEB	M3003E
QIAgility robotic workstation	Qiagen	9001908
Rotor-Disc 100	Qiagen	981311
Rotor-Disc Heat Sealer	Qiagen	9019725
Rotor-Disc Heat Sealing Film	Qiagen	981601
Rotor-Gene Q	Qiagen	9001560
Deposited data		
R script for WGS data processing	This study	10.5281/zenodo.14793122
AlphaFold 3 protein models	This study	10.5281/zenodo.14793919

Oligonucleotides		
See Table S4		
Recombinant DNA		
See Table S3		
Software and algorithms		
CLC Genomics Workbench	Qiagen	
CorelDRAW® Graphics Suite	Alludo	
Fiji	ImageJ	Schindelin *et al.* (2012)[89]
Microsoft Office Suite	Microsoft	
NIS-Elements	Nikon	
Primer3Plus	Online tool	Untergasset *et al.* (2007)[90]
Pymol Molecular Graphics	Schrödinger, Inc.	Delano (2002)[91]
Rotor-Gene Q software v2.0.2	Qiagen	
Rsamtools	Bioconductor	
RStudio Desktop	Posit	

Experimental model and details

The following bacterial organisms were used: *E. coli* and *B. subtilis.* Unless otherwise stated in method details, strains were grown at 37°C using nutrient agar (NA) or lysogeny broth (LB: 10 g/L tryptone, 10 g/L NaCl, 5 g/L yeast extract) for routine selection and maintenance of bacterial strains. Supplements were added as required: ampicillin (100 µg/ml), erythromycin (1 µg/ml) in conjunction with lincomycin (25 µg/ml), chloramphenicol (5 µg/ml), kanamycin (5 µg/ml), spectinomycin (50 µg/ml), zeocin (10 µg/ml), xylose (1% w/v) and IPTG (0.05 mM, 0.1 mM or 1 mM).

Method details

Bacterial strains

Bacterial strains used in this study are listed in Table S2.

E. coli plasmid construction

E. coli transformations for constructs harbouring *priA* were performed in CW198 via heat-shock following the Hanahan method[92] and propagated in LB with appropriate antibiotics at 37°C. DH5α [*F- Φ80lacZΔM15 Δ(lacZYA-argF) U169 recA1 endA1 hsdR17(rk-, mk+) phoA supE44 thi-1 gyrA96 relA1 λ-*] was used for other plasmids construction. Plasmids were purified using QIAprep spin miniprep kits and recombinant DNA confirmed by sequencing (Table S3). Descriptions, where necessary, are provided below.

pCW367, pCW368, pCW478, pCW479, pCW510, pCW717, pCW734, pCW736 and pCW850 were generated by Quickchange mutagenesis using mutagenic primer pairs containing an overlap of 10-15 bp. PCR products were treated with DpnI for at least 3 hours to digest template DNA and 10 µl were used for *E. coli* transformation.

pCW300, pCW301, pCW327, pCW460, pCW471, pCW472, pCW575, pCW734, pCW736 and pCW766 were generated by Gibson assembly using the NEB Hi-Fi cloning kit according to manufacturer instructions following purification of individual PCR fragments using QIAquick PCR purification kits.

Linear recombinant DNA assembly

For recombinant DNA assembly without *E. coli* propagation, pCW573, pCW574, pCW577, pCW578, pCW605, pCW640, pCW672, pCW702, pCW720, pCW732, pCW758, pCW759, pCW760, pCW777, pCW779, pCW781, pCW783, pCW785, pCW802, pCW803, pCW804, pCW809, pCW834, pCW848, pCW854, pCW855, pCW857 and pCW859 were assembled linearly using a multistep *in vitro* assembly process followed by nested PCR amplification prior to *B. subtilis* transformation. Briefly, individual PCR fragments corresponding to homology regions and insert DNA were amplified, purified and DNA ends ligated using the NEB Hi-Fi cloning kit. Raw Gibson assembly products were then amplified using nested primer pairs annealing towards the end of homology regions and PCR products were used for *B. subtilis* transformation. Following isolation of *B. subtilis* colonies resistant to the appropriate antibiotic markers, genomic DNA was extracted using the DNeasy blood and tissue kit, regions corresponding to recombinant DNA were amplified via PCR using

oligonucleotides annealing outside homology fragments to ensure double crossover had occurred and results were confirmed via PCR product sequencing. Note that CW2045 and derivatives harbour the additional *addA*^{D682E} mutation necessary to propagate *addB*^{D961A}-*addA*^{D1172A} in live cells, which is surface exposed and structurally unlikely to impact AddAB end-processing activities (Fig. S12E).

B. subtilis strain construction

Transformation of competent *B. subtilis* cells was performed using an optimized two-step starvation procedure as previously described[93]. Briefly, recipient strains were grown overnight at 37°C in transformation medium (Spizizen salts: 0.2% w/v ammonium sulphate, 1.4% w/v dipotassium phosphate, 0.6% w/v potassium phosphate, 0.1% w/v tri-sodium citrate, 0.02% w/v magnesium sulphate supplemented with 1 µg/ml ammonium iron(III) citrate, 6 mM $MgSO_4$, 0.5% w/v glucose, 0.02 mg/ml tryptophan and 0.02% w/v casein peptone) supplemented with IPTG where required. Overnight cultures were diluted 1:20 into fresh transformation medium supplemented with IPTG where required and grown at 37°C for 2.5-3 hours with continual shaking. An equal volume of prewarmed starvation medium (Spizizen salts supplemented with 6 mM $MgSO_4$ and 0.5% w/v glucose) was added and the culture was incubated at 37°C for two hours with continual shaking. DNA was added to 350 µl cells and the mixture was incubated at 37°C for one hour with continual shaking. 20-200 µl of each transformation was plated onto selective media supplemented with IPTG where required and incubated at 37°C for 24-48 hours. Results were validated by propagating cells on relevant antibiotic markers and sequencing.

Spot titre assays

Cells were grown in LB overnight in the presence of 0.5% w/v glucose. Overnight cultures were diluted in fresh LB medium using 10-fold serial dilutions and 5 µL aliquots were spotted onto NA plates with or without xylose. NA plates were supplemented with IPTG when required as indicated on individual figure panels. All plates were incubated for 24 hours or up

603 to 48 hours when indicated. Experiments were performed independently at least three times
604 and representative data are shown.
605
606 *Immunoblot analyses*
607 Cultures were grown overnight in LB and diluted 1:100 in fresh medium the next morning.
608 Diluted cells were grown to an absorbance at 600 nm (A_{600}) of 0.2-0.3, induced with 1% w/v
609 xylose or 1 mM IPTG where required and further incubated for one hour. Cells were
610 harvested using centrifugation, resuspended in 1x PBS supplemented with one tenth of a
611 peptidase inhibitor tablet and sonicated (40 amp) twice for 12 seconds with 3 second pulses
612 at 4°C. Samples were adjusted to 1X LDS buffer and 125 mM DTT, fixed for 5 minutes at
613 95°C and centrifuged for 2 minutes prior to loading the supernatant on polyacrylamide gels.
614 Proteins were separated by electrophoresis using NuPAGE 4-12% Bis-Tris gradient gels run
615 in MES SDS buffer and transferred to methanol-activated Hybond-P PVDF membranes
616 using Wypall X60 cloths for blotting in a semi-dry apparatus (Bio-rad Trans-Blot Turbo,
617 transfer buffer: 300 mM Tris-HCl, 300 mM glycine, 140 mM tricine, 0.05% w/v SDS, 2.5 mM
618 EDTA). Membranes were washed twice using PBST (1X PBS supplemented with 0.1% v/v
619 Tween-20) prior to blocking for 90 minutes at room temperature (blocking buffer: PBST
620 supplemented with 7.5% w/v milk). Individual polypeptides were probed using the following
621 primary antibodies diluted in blocking buffer following overnight incubation at 4°C: anti-Cas9
622 (1:1000), anti-FtsZ (1:5000), anti-PriA (1:1000), anti-SSB (1:1000) and anti-mNeonGreen
623 (1:1000). Detection was performed with anti-rabbit (PriA, SSB), anti-sheep (FtsZ) or anti-
624 mouse (Cas9, mNeonGreen) horseradish peroxidase-linked secondary antibodies in
625 combination with the Clarity ECL substrate using an ImageQuant LAS 4000 mini digital
626 imaging system. Detection of Cas9, FtsZ, PriA, SSB and mNeonGreen was within a linear
627 range. Experiments were independently performed at least twice and representative data
628 are shown.
629
630 *Whole genome sequencing*

Cells were grown in rich chemically defined medium (RCDM: Spizizen salts supplemented with 1 µg/ml ammonium iron(III) citrate, 0.1 mM $CaCl_2$, 0.13 mM $MnSO_4$, 6 mM $MgSO_4$, 0.5% w/v glucose, 0.1% w/v glutamate, 0.02 mg/ml tryptophan and 0.02% w/v casein peptone) overnight and diluted 1:100 in fresh RCDM the next morning. Diluted cells were grown to an absorbance at 600 nm (A_{600}) of 0.2-0.3, induced with 1% w/v xylose and further incubated for one hour. Growth was arrested by adding 0.05% w/v sodium azide to cultures followed by vigorous mixing, cells were collected by centrifugation, the supernatant discarded, and pellets were flash frozen in liquid nitrogen before genomic DNA extraction using the DNeasy blood and tissue kit and a final elution volume of 50 µl in ultrapure water. Individual gDNA libraries were prepared using the DNA Prep tagmentation kit and pre-paired i5/i7 indices prior to pooling and DNA quantification with the 1X dsDNA high sensitivity kit using a Qubit instrument. Pooled libraries were diluted to 100 pM in resuspension buffer and 20 µl were loaded onto iSeq 100 i1 Reagent v2 sequencing chips for whole-genome sequencing using an iSeq100 sequencer.

Following whole-genome sequencing and demultiplexing embedded within the iSeq100 indexed sequencing workflow, .FASTQ files were extracted and loaded onto the CLC Genomics Workbench for initial data processing. Paired .FASTQ files were mapped onto the *B. subtilis* Δ6 reference genome using the 'Map Reads to Reference' function and a .BAM file was created from mapped sequencing reads for each sequenced genome. An in-house script written in R using the Rsamtools library was employed to deconvolute .BAM files to validate even read distribution for sense/antisense strands prior to calculating density coverage and extracting cumulated densities per chromosome position.

Fluorescence microscopy

Strains were grown overnight at 37°C in RCDM and the following day, cultures were diluted 1:100 into fresh imaging medium (RCDM where glucose is replaced by 0.5% v/v glycerol) in the presence of 0.1 mM IPTG for induction of mNeonGreen-RecA expression where required. Cells were allowed to grow to an A_{600} of 0.3, induced with 1% w/v xylose and

further incubated for 90 minutes. DAPI (5 µg/ml) and Nile red (1 µg/ml) stains were used to visualise the nucleoid and cell membrane following a 10 minute incubation on a benchtop incubator prior to imaging.

Cells were mounted on ~1.25% agar pads (in sterile ultrapure water) and a 0.13- to 0.17-mm glass coverslip was placed on top. Microscopy was performed on an inverted epifluorescence microscope (Nikon Ti) fitted with a Plan Apochromat Objective 100x/1.40 NA Oil Ph3. Light was transmitted from a CoolLED pE-300 white light source through a Sutter Instruments liquid light guide and images were collected using a Photometrics Prime camera. Chroma fluorescence filter sets were used with 100 ms GFP, 250 ms DAPI and 50 ms mCherry exposure times at 100% LED power. Digital images were acquired using NIS Elements and analysed via the Fiji software[89]. Quantification of mNeonGreen-RecA features was manually curated from the count of 100 individual cells. All experiments were independently performed at least twice and representative data are shown.

Chromatin immunoprecipitation

Chromatin immunoprecipitation (ChIP) was performed as previously described with minor modifications[32]. Strains were grown overnight at 37°C in RCDM and the following day, cultures were diluted 1:100 into fresh medium and allowed to grow to an A_{600} of 0.2-0.3. Cells were induced with 1% w/v xylose and further incubated for one hour prior to ChIP. Samples were adjusted to 1X PBS and crosslinked with 1% v/v formaldehyde for 10 minutes on a roller at room temperature, then quenched with 0.1 M glycine. Cells were pelleted at 4°C, washed three times with ice-cold 1X PBS (pH 7.3), frozen in liquid nitrogen and stored at -80°C. Frozen cell pellets were resuspended in 500 µl of lysis buffer (50 mM NaCl, 10 mM Tris-HCl pH 8.0, 20% w/v sucrose, 10 mM EDTA, 100 µg/ml RNase A, one quarter of a peptidase inhibitor tablet, 4 mg/ml lysozyme) and incubated at 37°C for 30 min to degrade the cell wall. Protoplasts were supplemented with 500 µl of immunoprecipitation buffer (300 mM NaCl, 100 mM Tris-HCl pH 7.0, 2% v/v Triton X-100, one quarter of a peptidase inhibitor tablet) to lyse cells and the mixture was incubated at 37°C for a further 10 minutes before

cooling on ice for 5 minutes. Lysis and immunoprecipitation buffer volumes were multiplied by the number of antibodies to probe per sample. DNA samples were sonicated (40 amp) three times for 2 minutes at 4°C to obtain an average fragment size of 500 to 1000 base pairs. Cell debris were removed by centrifugation at 4°C and the supernatant transferred to a fresh Eppendorf tube. To determine the relative amount of DNA immunoprecipitated compared to the total amount of DNA, 100 µl of supernatant was removed, treated with 0.5 mg/ml pronase at 37°C for four hours then stored on ice. To immunoprecipate protein-DNA complexes, 800 µl of the remaining supernatant was incubated with individual antibodies (2 µl anti-SSB, 2 µl anti-PriA, 2 µl anti-DnaD, 2 µl anti-DnaB, 2 µl anti-DnaI, 2 µl anti-DnaC, 2 µl anti-mNeonGreen or 4 µl anti-His) for 90 minutes at room temperature. 750 µg of protein G Dynabeads were equilibrated by washing with bead buffer (1X PBS, 0.01% v/v Tween 20), resuspended in 25 µl of bead buffer and incubated with the sample supernatant for 1 hour at room temperature. Immunoprecipitated complexes were collected by applying the mixture to a magnet and washed with the following buffers in the respective order: 0.5X immunoprecipitation buffer for 15 min, 0.5X immunoprecipitation buffer supplemented with 500 mM NaCl for 15 min, stringent wash buffer (250 mM LiCl, 10 mM Tris-HCl pH 8.0, 0.5% v/v Igepal, 0.5% w/v sodium deoxycholate, 10 mM EDTA) for 20 min. Finally, protein-DNA complexes were washed a further three times with TET buffer (10 mM Tris-HCl pH 8.0, 1 mM EDTA, 0.01% v/v Tween 20) and resuspended in 100 µl of TEN buffer (10 mM Tris-HCl pH 8.0, 1 mM EDTA, 300 mM NaCl). Formaldehyde crosslinks of both the immunoprecipitate and total DNA were reversed by incubation at 65°C for 18 hours in the presence of 1 mg/ml proteinase K. DNA was then removed from the magnetic beads, cleaned using QIAquick PCR purification columns and used for quantitative PCR analyses.

Quantitative PCR

Quantitative PCR (qPCR) was performed using the Luna qPCR master mix to measure relative amounts of DNA bound by SSB, PriA, DnaD, DnaB, DnaI, DnaC, mNeonGreen-AddA, mNeonGreen-AddB, His-RecO and His-RecA at specific genomic locations (e.g. near

the nick site located at -90° on the chromosome or the origin *oriC* compared to a control site located at +90° on the chromosome). All PCR reactions were assembled using the QIAgility robotic workstation in 20 µl reaction volumes in a Rotor-Disc 100 and qPCRs were run on a Rotor-Gene Q instruments. Standard curves were obtained using the Rotor-Gene Q software to calculate the efficiency of each primer pair, which varied ~5% between sets. Oligonucleotides were designed to amplify specific genomic regions using the Primer3Plus tool[90], were typically 20-25 bases in length (Table S4) and amplified a ~100 bp PCR product. Individual fold enrichment ratios were obtained as follows: first, every Ct value was converted to $1/2^{Ct}$ and technical triplicates were averaged to generate a single enrichment value; second, genomic location specific enrichment was normalised by corresponding values obtained at +90° on the chromosome. Error bars indicate the standard error of the mean for three biological replicates.

Protein structure prediction and representation

Protein models for SSB:ssDNA and SSB:RecO were generated using AlphaFold 3 and polypeptides corresponding to individual protein entities as input[94]. Main and alternative models were manually examined and Model 0 was chosen to highlight key features using the Pymol Molecular Graphics 2.1 software[91]. Structural highlights of the AddAB complex were derived from the crystal structure PDB: 4CEH[95].

FIGURE TITLES AND LEGENDS

Figure 1. Single-strand discontinuities arrest DNA synthesis and generate DSBs.

(A) Diagram illustrating the impact of leading and lagging strand discontinuities on a replication fork, with the bacterial replicative helicase translocating along the template for the lagging strand.

(B) Genetic system employed to create a site-specific single-strand discontinuity in the *B. subtilis* chromosome. Black boxes correspond to antibiotic resistance markers, pink to Cas9 variants and green to sgRNA. Chromosome annotations refer to the replication origin (0), terminus (180) and sgRNA target sequence (yellow box).

(C) Spot titre analysis of strains engineered to express (+xylose) either nCas9 or dCas9. Individual sgRNAs were designed to target both strands at loci located at either -90° (top panel) or +90° (bottom panel).

(D) MFA using whole genome sequencing of strains engineered to express either nCas9 or dCas9. Individual sgRNAs were designed to target both strands at loci located at either -90° (left panel) or +90° (right panel). The frequency of sequencing reads was plotted against genome position.

(E) Representative fluorescence microscopy images of the DSB reporter mNG-RecA in strains engineered to express (+xylose) either nCas9 or dCas9 (sgRNAs target -90°). Fluorescent RecA organises into bundles in the presence of DSBs. Green signal corresponds to mNG-RecA fluorescence, grey scale images show corresponding phase contrast images.

(F) Quantification of fluorescence microscopy images of the DSB reporter mNG-RecA in strains engineered to express (+xylose) either nCas9 or dCas9 (sgRNA target -90°). Detection of spots and bundles corresponds to distinct foci or filament-like structures annotated in panel (E). Error bars indicate the standard error of the mean.

Figure 2. Replication restart is necessary to resume DNA synthesis following replisome inactivation at a single-strand discontinuity.

(A) Diagram illustrating genomic locations probed via ChIP-qPCR at loci located at either -90° or +90°. The sgRNA targeted Cas9 protein variants to the locus at -90°. The enrichment signal at the +90° locus was used for fold change normalisation. Lagging strand and leading strand templates are represented in black and grey lines, respectively (numbers refer to polarity). Blue arrows indicate leading strand synthesis and red arrows indicate lagging strand synthesis.

(B-F) ChIP-qPCR analyses of helicase (DnaC) and replication restart proteins (PriA, DnaD, DnaB, DnaI) in strains engineered to express either nCas9 or dCas9. The sgRNAs targeted Cas9 proteins to a locus located at -90° and fold change was normalised to enrichment values obtained at the +90° locus. Error bars indicate the standard error of the mean.

(G) Diagram illustrating the fate of helicase (red hexagon) upon encountering a single-strand discontinuity in either the leading or lagging strand template.

(H) MFA using whole genome sequencing in strains engineered to express lower levels of sgRNAs and Cas9 proteins (weak nicking system). The frequency of sequencing reads was plotted against genome position.

(I) Genetic system employed to express low levels of PriA in a background encoding the weak nicking system.

(J) Spot titre analysis of strains with a low level of PriA engineered to express nCas9 (+xylose). sgRNAs were targeted to a locus at -90°.

(K) MFA using whole genome sequencing in strains with a low level of PriA engineered to express (+xylose) nCas9. The frequency of sequencing reads was plotted against genome position.

Figure 3. The repair of single-strand discontinuities requires homologous recombination.

(A) Spot titre analysis of homologous recombination mutants in strains engineered to express (+xylose) nCas9. sgRNAs were targeted to a locus at -90° and control strains correspond to parental strains.

(B) MFA using whole genome sequencing of homologous recombination mutants in strains engineered to express nCas9. The frequency of sequencing reads was plotted against genome position.

(C) Diagram illustrating proposed molecular events required for homologous recombination to repair the DSB created after a replication fork encounters a single-strand discontinuity in the leading strand template.

Figure 4. The SSB-CTT is essential to recruit RecO following replisome inactivation at a single-strand discontinuity.

(A) ChIP-qPCR analyses of SSB in strains engineered to express nCas9. The sgRNAs targeted nCas9 to a locus located at -90° and fold change was normalised to enrichment values obtained at the +90° locus. Error bars indicate the standard error of the mean.

(B) ChIP-qPCR analyses of SSB in strains with homologous recombination mutants engineered to express nCas9. qPCR primers amplified either a site located at -3 kb from the sgRNA target (-90°) or a control locus (+90°) used for normalisation. Error bars indicate the standard error of the mean.

(C) Spot titre analysis of SSB variants in strains engineered to express (+xylose) nCas9. Top panel shows the genetic system employed in this experiment. sgRNAs were targeted to a locus at -90°.

(D) MFA using whole genome sequencing in strains with SSB variants engineered to express nCas9. The frequency of sequencing reads was plotted against genome position.

(E) ChIP-qPCR analyses of SSB, His-RecO and His-RecA proteins in strains engineered to express nCas9. qPCR primers amplified either a site located at -3 kb from the sgRNA target (-90°) or a control locus (+90°) used for normalisation. Error bars indicate the standard error of the mean.

(F) ChIP-qPCR analyses of His-RecA in strains with homologous recombination mutants engineered to express nCas9. Top panel shows the genetic system employed in this experiment. qPCR primers amplified either a site located at -3 kb from the sgRNA target (-

90°) or a control locus (+90°) used for normalisation. Error bars indicate the standard error of the mean.

Figure 5. DNA end resection via AddAB is not required to recruit SSB following replisome inactivation at a single-strand discontinuity.

(A) MFA using whole genome sequencing in a Δ*recG* mutant strain engineered to express nCas9. The frequency of sequencing reads was plotted against genome position (same data as in Fig. 3B Δ*recG* panel). A region flanking the sgRNA binding site is enlarged.

(B) Diagram illustrating incorrect helicase reloading leading to reverse restart on a repaired replication fork in a Δ*recG* mutant. Helicase is shown as a red hexagon and RecG is shown in green; protein movement is indicated by colour-corresponding arrows. Lagging strand and leading strand templates are represented in black and grey lines, respectively. Blue arrows indicate leading strand synthesis.

(C) ChIP-qPCR analyses of mNG-AddA and mNG-AddB in strains engineered to express nCas9. Left panel shows the genetic system employed in this experiment. The sgRNAs targeted nCas9 to a locus located at -90° and fold change was normalised to enrichment values obtained at the +90° locus. Error bars indicate the standard error of the mean.

(D) Spot titre analysis in strains with either $AddA^{\Delta HEL}$, $AddA^{\Delta NUC}$ or $AddB^{\Delta NUC}$ engineered to express (+xylose) nCas9. sgRNAs were targeted to a locus at -90° and control strains correspond to parental strains.

(E) MFA using whole genome sequencing of strains with either $AddA^{\Delta HEL}$ or $AddA^{\Delta NUC}$/$AddB^{\Delta NUC}$ engineered to express nCas9. The frequency of sequencing reads was plotted against genome position. Top panel shows the genetic system employed in this experiment.

(F) ChIP-qPCR analyses of SSB in strains with AddA and AddB variants engineered to express nCas9. Alleles refer to wild-type (WT), knockouts (Δ), and point mutations inactivating nuclease (ΔNUC) or helicase (ΔHEL) activities. qPCR primers amplified either a

site located at -3 kb from the sgRNA target (-90°) or a control locus (+90°) used for normalisation. Error bars indicate the standard error of the mean.

Figure 6. RecG is dispensable when DSB processing degrades the strand with a 5′-end.

(A) Diagram illustrating differential resection of a DSB in the presence of either the AddA or AddB nuclease activity. Leading and lagging strand templates are indicated by grey and blue lines, respectively (numbers indicate polarity). Dotted lines indicate nuclease cleavage.

(B) Genetic system employed to investigate the role of RecG in DSB repair following replisome inactivation at a single-strand discontinuity.

(C) Spot titre analysis in a Δ*recG* mutant strain with either AddA$^{\Delta NUC}$ or AddB$^{\Delta NUC}$ engineered to express (+xylose) nCas9. sgRNAs were targeted to a locus at -90° and control strains correspond to parental strains encoding the weak nicking system.

(D) Diagram illustrating differential helicase reloading events on a repaired replication fork when AddA or AddB nuclease activity is inactivated in the absence of RecG. Helicase is shown as a red hexagon and PriA in yellow; protein movement is indicated by colour-corresponding arrows. Lagging strand and leading strand templates are represented in black and grey lines, respectively. Blue arrows indicate leading strand synthesis.

Figure 7. Model for DSB repair and helicase reloading following replisome inactivation at a single-strand discontinuity.

Revised model illustrating molecular events that are required or dispensable for homologous repair of a DSB created after a replication fork encounters a single-strand discontinuity located on either the leading or lagging strand template.

SUPPLEMENTARY FIGURE TITLES AND LEGENDS

Supplementary Figure 1. Impact of Cas9 variants on *B. subtilis* cell growth.

(A) Spot titre analysis of strains expressing (+ xylose) either $Cas9^{D10A}$ nickase, $Cas9^{H840A}$ nickase, or $Cas9^{D10A\text{-}H840A}$ catalytically inactive nuclease in the presence of the same sgRNA. Left panel shows the genetic system employed in this experiment. sgRNAs were targeted to a locus at -90°.

(B) Immunoblot of Cas9 variants in the presence of a sgRNA targeted to a locus at -90°.. Cas9 proteins were induced (+xylose) during the exponential growth phase for 1 hour before cells were harvested for protein extraction. The tubulin homolog FtsZ was used as a loading control.

(C) Spot titre analysis of a strain expressing (+ xylose) the $Cas9^{D10A}$ nickase with different sgRNAs targeting different locations along the left chromosome arm.

(D) Spot titre analysis of strains expressing (+ xylose) the $Cas9^{D10A\text{-}H840A}$ catalytically inactive nuclease. Left panel shows the genetic system employed in this experiment for sgRNAs targeted to a locus at either -90° or +90°.

Supplementary Figure 2. MFA using whole genome sequencing of the parental strain *B. subtilis* Δ6.

The frequency of sequencing reads was plotted against genome position. Note that chromosome physical boundaries indicated on x-axis may not represent termination events occurring in the cell (*terminus* region highlighted in yellow).

Supplementary Figure 3. Live cell fluorescence microscopy using the mNG-RecA reporter of DNA damage.

(A) Phase contrast image and fluorescence signal from the mNG-RecA reporter in wild-type *B. subtilis* under standard laboratory growth conditions.

(B) Representative fluorescence microscopy images of mNG-RecA in strains engineered to express either nCas9 or dCas9 (sgRNA target -90°). Fluorescent RecA organises into

bundles in the presence of DSBs. Green signal corresponds to mNG-RecA fluorescence, grey scale images show corresponding phase contrast images. Cas9 proteins were induced (+xylose) during the exponential growth phase for 1 hour before cells were collected for imaging.

Supplementary Figure 4. The replicative helicase DnaC is recruited near a single-strand discontinuity.

ChIP-qPCR analyses of helicase (DnaC) in strains engineered to express either nCas9 or dCas9. The sgRNAs targeted Cas9 proteins to a locus located at -90°. The replication origin *oriC* was used as positive control and fold change was normalised to enrichment values obtained at the +90° locus. Error bars indicate the standard error of the mean.

Supplementary Figure 5. The weak nicking system does not arrest cell growth.

(A) Schematic showing differences between the strong and weak nicking systems to introduce a single-strand discontinuity.

(B) Spot titre analysis of strains expressing (+ xylose) the strong of weak nicking system in the presence of the same sgRNA. Control indicates a strain encoding the $Cas9^{D10A\text{-}H840A}$ catalytically inactive nuclease. sgRNAs targeted to a locus located at -90°.

(C) Live cell fluorescence microscopy using nucleoid and membrane stains in strains expressing either the strong or the weak nicking system. Grey scale images correspond to phase contrast, blue signal corresponds to DAPI staining (nucleoid), red signal corresponds to Nile red staining (membrane) and merge corresponds to DAPI/Nile red composite images. Cas9 proteins were induced (+xylose) during the exponential growth phase for 90 minutes before cells were collected for imaging.

Supplementary Figure 6. Complementation system employed to investigate PriA essentiality following replisome inactivation at single-strand discontinuities.

(A) Genetic system employed for *priA* complementation via the IPTG inducible *priA-ssrA* cassette placed at an ectopic locus in wild-type *B. subtilis*.

(B) Spot titre analysis of strains expressing (+ IPTG) the *priA-ssrA* complementation system.

(C) Immunoblot of PriA variants expressed at variable IPTG concentrations. The tubulin homolog FtsZ was used as a loading control.

(D) Spot titre analysis of strains with a very low or high level of PriA engineered to express nCas9 (+xylose). sgRNAs were targeted to a locus at -90°.

Supplementary Figure 7. DSB repair following replisome inactivation at a single-strand discontinuity is achieved via homologous recombination.

(A) Spot titre analysis of homologous recombination mutants in strains engineered to express (+xylose) nCas9. sgRNAs were targeted to a locus at -90° and control strains correspond to parental strains. Plates were the same as shown in Fig. 3A when incubated up to 48 hours.

(B) Spot titre analysis of homologous recombination mutants complemented with epitope-tagged ectopic gene copies in strains engineered to express (+xylose) nCas9. sgRNAs were targeted to a locus at -90° and control strains correspond to parental strains.

(C) Diagram illustrating proposed molecular events required for homologous recombination to repair the DSB created after a replication fork encounters a single-strand discontinuity in the lagging strand template.

Supplementary Figure 8. DSB repair following replisome inactivation at a single-strand discontinuity relies on a minimal set of non-essential genes.

(A-D) Spot titre analysis of DNA repair mutants grouped by known/proposed functions in strains engineered to express (+xylose) nCas9. sgRNAs were targeted to a locus at -90° and control strains correspond to parental strains.

Supplementary Figure 9. Complementation system employed to investigate the function of the SSB-CTT following replisome inactivation at single-strand discontinuities.

(A) Schematic of SSB primary structure with corresponding functions. Numbers indicate amino acid residue boundaries between the N-terminal domain (NTD), C-terminal domain (CTD) and C-terminal tail (CTT).

(B) Model *of B. subtilis* SSB homotetramer in the presence of single-strand DNA (AlphaFold 3). The black backbone corresponds to a homopolymer of 60 thymidine bases and SSB-CTT residues are highlighted in red.

(C) Genetic system employed for *ssbA* complementation via an IPTG inducible cassette placed at an ectopic locus in wild-type *B. subtilis*.

(D) Spot titre analysis of strains expressing (+ IPTG) *ssbA* variants using the complementation system.

(E) Immunoblot of SSB variants expressed using the *ssbA* complementation system. The tubulin homolog FtsZ was used as a loading control.

(F) Genetic system employed to express SSB variants in a background encoding the weak nicking system.

(G) Diagram illustrating potential essential interactions of the SSB-CTT.

(H) Model of a complex between an SSB homotetramer and RecO from *B. subtilis* (AlphaFold 3). Cyan corresponds to SSB with CTT residues coloured in red and RecO is displayed in beige.

Supplementary Figure 10. Traditional homologous repair models require end resection to generate 3′-tailed DNA.

Diagram illustrating textbook molecular events required for homologous recombination to repair the DSB created after a replication fork encounters a single-strand discontinuity in either the leading or the lagging strand template.

Supplementary Figure 11. PriA recognises D-loops where the 3′-OH group of the nascent leading strand abuts the fork junction.

Diagram illustrating the substrate recognised by PriA to orchestrate correct helicase reloading.

Supplementary Figure 12. End-processing activities required following replisome inactivation at a single-strand discontinuity.

(A) Immunoblot of AddA variants expressed from *mNG* epitope-tagged fusions. The tubulin homolog FtsZ was used as a loading control.

(B-C) MFA using whole genome sequencing of strains with either AddA$^{\Delta HEL}$, AddA$^{\Delta NUC}$ or AddB$^{\Delta NUC}$ engineered to express nCas9. The frequency of sequencing reads was plotted against genome position. AddA$^{\Delta HEL}$ samples were the same as shown in Fig. 5E.

(D) Crystal structure of the *B. subtilis* AddAB complex with locations of catalytic sites and the AddA^{D682} residue indicated (PDB template: 4CEH). The black backbone corresponds to DNA,

AddA is displayed in orange and AddB in beige.

SUPPLEMENTAL INFORMATION

Documents S1-S12. Figures S1-S12, related to main Figures.

Table S1. Excel file too large to fit in a PDF containing the list of repair gene knockouts tested in the genetic screen, related to Figures 3 and S8.

Table S2. Excel file too large to fit in a PDF containing genotypes from strains generated in this study, related to the Key resources table.

Table S3. Excel file too large to fit in a PDF containing genotypes and sequences of recombinant DNA used to construct strains in this study, related to the Key resources table and Table S2.

Table S4. Excel file too large to fit in a PDF containing oligonucleotide sequences used for qPCR in this study, related to the Key resources table.

REFERENCES

1. Murray, C.J.L., Ikuta, K.S., Sharara, F., Swetschinski, L., Aguilar, G.R., Gray, A., Han, C., Bisignano, C., Rao, P., Wool, E., et al. (2022). Global burden of bacterial antimicrobial resistance in 2019: a systematic analysis. Lancet *399*, 629-655. 10.1016/S0140-6736(21)02724-0.
2. Butler, M.S., Vollmer, W., Goodall, E.C.A., Capon, R.J., Henderson, I.R., and Blaskovich, M.A.T. (2024). A Review of Antibacterial Candidates with New Modes of Action. Acs Infect Dis *10*, 3440-3474. 10.1021/acsinfecdis.4c00218.
3. Dwyer, D.J., Kohanski, M.A., and Collins, J.J. (2009). Role of reactive oxygen species in antibiotic action and resistance. Curr Opin Microbiol *12*, 482-489. 10.1016/j.mib.2009.06.018.
4. Charbon, G., Bjorn, L., Mendoza-Chamizo, B., Frimodt-Moller, J., and Lobner-Olesen, A. (2014). Oxidative DNA damage is instrumental in hyperreplication stress-induced inviability of. Nucleic Acids Research *42*, 13228-13241. 10.1093/nar/gku1149.
5. Kohanski, M.A., Dwyer, D.J., Hayete, B., Lawrence, C.A., and Collins, J.J. (2007). A common mechanism of cellular death induced by bactericidal antibiotics. Cell *130*, 797-810. 10.1016/j.cell.2007.06.049.
6. Fan, X.Y., Tang, B.K., Xu, Y.Y., Han, A.X., Shi, K.X., Wu, Y.K., Ye, Y., Wei, M.L., Niu, C., Wong, K.W., et al. (2018). Oxidation of dCTP contributes to antibiotic lethality in stationary-phase mycobacteria. Proc Natl Acad Sci U S A *115*, 2210-2215. 10.1073/pnas.1719627115.
7. Lenhart, J.S., Schroeder, J.W., Walsh, B.W., and Simmons, L.A. (2012). DNA repair and genome maintenance in *Bacillus subtilis*. Microbiol Mol Biol Rev *76*, 530-564. 10.1128/MMBR.05020-11.
8. Gaimster, H., Stevens, D., Hubbard, J., Mickiewicz, K., Murray, H., and Winterhalter, C. (2024). Conflicts between the DNA replication and repair machineries promote cell death in Gram-positive bacteria. bioRxiv, 2024.2010.2024.619994. 10.1101/2024.10.24.619994.
9. Lindahl, T., and Wood, R.D. (1999). Quality control by DNA repair. Science *286*, 1897-1905. DOI 10.1126/science.286.5446.1897.
10. Michel, B., Sinha, A.K., and Leach, D.R.F. (2018). Replication Fork Breakage and Restart in Escherichia coli. Microbiol Mol Biol Rev *82*. 10.1128/MMBR.00013-18.
11. Kuzminov, A. (2001). Single-strand interruptions in replicating chromosomes cause double-strand breaks. Proc Natl Acad Sci U S A *98*, 8241-8246. 10.1073/pnas.131009198.
12. Kornberg, A., and Baker, T.A. (1992). DNA replication, 2 Edition (W.H. Freeman and Co).
13. O'Donnell, M. (2006). Replisome architecture and dynamics in Escherichia coli. J Biol Chem *281*, 10653-10656. 10.1074/jbc.R500028200.
14. Kim, D.E., Narayan, M., and Patel, S.S. (2002). T7 DNA helicase: a molecular motor that processively and unidirectionally translocates along single-stranded DNA. J Mol Biol *321*, 807-819. 10.1016/s0022-2836(02)00733-7.
15. Xu, Z.Q., and Dixon, N.E. (2018). Bacterial replisomes. Curr Opin Struct Biol *53*, 159-168. 10.1016/j.sbi.2018.09.006.
16. Fernandez, A.J., and Berger, J.M. (2021). Mechanisms of hexameric helicases. Crit Rev Biochem Mol Biol *56*, 621-639. 10.1080/10409238.2021.1954597.
17. Beattie, T.R., Kapadia, N., Nicolas, E., Uphoff, S., Wollman, A.J., Leake, M.C., and Reyes-Lamothe, R. (2017). Frequent exchange of the DNA polymerase during bacterial chromosome replication. Elife *6*. 10.7554/eLife.21763.
18. Graham, J.E., Marians, K.J., and Kowalczykowski, S.C. (2017). Independent and Stochastic Action of DNA Polymerases in the Replisome. Cell *169*, 1201-1213 e1217. 10.1016/j.cell.2017.05.041.

19. Yeeles, J.T., and Marians, K.J. (2011). The Escherichia coli replisome is inherently DNA damage tolerant. Science *334*, 235-238. 10.1126/science.1209111.
20. Vrtis, K.B., Dewar, J.M., Chistol, G., Wu, R.A., Graham, T.G.W., and Walter, J.C. (2021). Single-strand DNA breaks cause replisome disassembly. Mol Cell *81*, 1309-1318 e1306. 10.1016/j.molcel.2020.12.039.
21. Pavani, R., Tripathi, V., Vrtis, K.B., Zong, D., Chari, R., Callen, E., Pankajam, A.V., Zhen, G., Matos-Rodrigues, G., Yang, J., et al. (2024). Structure and repair of replication-coupled DNA breaks. Science *385*, eado3867. 10.1126/science.ado3867.
22. Jinek, M., East, A., Cheng, A., Lin, S., Ma, E.B., and Doudna, J. (2013). RNA-programmed genome editing in human cells. Elife *2*. ARTN e00471 10.7554/eLife.00471.
23. Xu, Y., Morrow, C.A., Laksir, Y., Holt, O.M., Taylor, K., Tsiappourdhi, C., Collins, P., Jia, S., Andreadis, C., and Whitby, M.C. (2025). DNA nicks in both leading and lagging strand templates can trigger break-induced replication. Mol Cell *85*, 91-106 e105. 10.1016/j.molcel.2024.10.026.
24. Lee, J., Lim, K., Kim, A., Mok, Y.G., Chung, E., Cho, S.I., Lee, J.M., and Kim, J.S. (2023). Prime editing with genuine Cas9 nickases minimizes unwanted indels. Nature Communications *14*. 10.1038/s41467-023-37507-8.
25. Peters, J.M., Colavin, A., Shi, H.D., Czarny, T.L., Larson, M.H., Wong, S., Hawkins, J.S., Lu, C.H.S., Koo, B.M., Marta, E., et al. (2016). A Comprehensive, CRISPR-based Functional Analysis of Essential Genes in Bacteria. Cell *165*, 1493-1506. 10.1016/j.cell.2016.05.003.
26. Westers, H., Dorenbos, R., van Dijl, J.M., Kabel, J., Flanagan, T., Devine, K.M., Jude, F., Seror, S.J., Beekman, A.C., Darmon, E., et al. (2003). Genome engineering reveals large dispensable regions in Bacillus subtilis. Mol Biol Evol *20*, 2076-2090. 10.1093/molbev/msg219.
27. Simmons, L.A., Grossman, A.D., and Walker, G.C. (2007). Replication is required for the RecA localization response to DNA damage in Bacillus subtilis. Proc Natl Acad Sci U S A *104*, 1360-1365. 10.1073/pnas.0607123104.
28. Lesterlin, C., Ball, G., Schermelleh, L., and Sherratt, D.J. (2014). RecA bundles mediate homology pairing between distant sisters during DNA break repair. Nature *506*, 249-253. 10.1038/nature12868.
29. Kidane, D., and Graumann, P.L. (2005). Dynamic formation of RecA filaments at DNA double strand break repair centers in live cells. J Cell Biol *170*, 357-366. 10.1083/jcb.200412090.
30. Smits, W.K., Goranov, A.I., and Grossman, A.D. (2010). Ordered association of helicase loader proteins with the Bacillus subtilis origin of replication in vivo. Mol Microbiol *75*, 452-461. 10.1111/j.1365-2958.2009.06999.x.
31. Michel, B., and Sandler, S.J. (2017). Replication Restart in Bacteria. J Bacteriol *199*. 10.1128/JB.00102-17.
32. Winterhalter, C., Pelliciari, S., Stevens, D., Fenyk, S., Marchand, E., Cronin, N.B., Soultanas, P., Costa, T.R.D., Ilangovan, A., and Murray, H. (2023). The DNA replication initiation protein DnaD recognises a specific strand of the Bacillus subtilis chromosome origin. Nucleic Acids Res *51*, 4322-4340. 10.1093/nar/gkad277.
33. Winterhalter, C., Stevens, D., Fenyk, S., Pelliciari, S., Marchand, E., Soultanas, P., Ilangovan, A., and Murray, H. (2022). SirA inhibits the essential DnaA:DnaD interaction to block helicase recruitment during Bacillus subtilis sporulation. Nucleic Acids Res. 10.1093/nar/gkac1060.
34. Matthews, L.A., and Simmons, L.A. (2020). Regulation of DNA Binding and High-Order Oligomerization of the DnaB Helicase Loader. J Bacteriol *202*. 10.1128/JB.00286-20.
35. Bruand, C., Farache, M., McGovern, S., Ehrlich, S.D., and Polard, P. (2001). DnaB, DnaD and DnaI proteins are components of the Bacillus subtilis replication restart primosome. Molecular Microbiology *42*, 245-255. DOI 10.1046/j.1365-2958.2001.02631.x.

36. Kaguni, J.M. (2011). Replication initiation at the Escherichia coli chromosomal origin. Curr Opin Chem Biol *15*, 606-613. 10.1016/j.cbpa.2011.07.016.
37. Kaplan, D.L. (2000). The 3'-tail of a forked-duplex sterically determines whether one or two DNA strands pass through the central channel of a replication-fork helicase. J Mol Biol *301*, 285-299. 10.1006/jmbi.2000.3965.
38. Griffith, K.L., and Grossman, A.D. (2008). Inducible protein degradation in Bacillus subtilis using heterologous peptide tags and adaptor proteins to target substrates to the protease ClpXP. Mol Microbiol *70*, 1012-1025. 10.1111/j.1365-2958.2008.06467.x.
39. Cox, M.M., Goodman, M.F., Kreuzer, K.N., Sherratt, D.J., Sandler, S.J., and Marians, K.J. (2000). The importance of repairing stalled replication forks. Nature *404*, 37-41.
40. Yasmin, T., Azeroglu, B., Cockram, C.A., and Leach, D.R.F. (2021). Distribution of Holliday junctions and repair forks during Escherichia coli DNA double-strand break repair. PLoS Genet *17*, e1009717. 10.1371/journal.pgen.1009717.
41. Sanchez, H., Kidane, D., Castillo Cozar, M., Graumann, P.L., and Alonso, J.C. (2006). Recruitment of Bacillus subtilis RecN to DNA double-strand breaks in the absence of DNA end processing. J Bacteriol *188*, 353-360. 10.1128/JB.188.2.353-360.2006.
42. Costes, A., Lecointe, F., McGovern, S., Quevillon-Cheruel, S., and Polard, P. (2010). The C-terminal domain of the bacterial SSB protein acts as a DNA maintenance hub at active chromosome replication forks. PLoS Genet *6*, e1001238. 10.1371/journal.pgen.1001238.
43. Ramos, C., Hernandez-Tamayo, R., Lopez-Sanz, M., Carrasco, B., Serrano, E., Alonso, J.C., Graumann, P.L., and Ayora, S. (2022). The RecD2 helicase balances RecA activities. Nucleic Acids Research *50*, 3432-3444. 10.1093/nar/gkac131.
44. Cárdenas, P.P., Carrasco, B., Soufo, C.D., César, C.E., Herr, K., Kaufenstein, M., Graumann, P.L., and Alonso, J.C. (2012). RecX Facilitates Homologous Recombination by Modulating RecA Activities. Plos Genetics *8*. ARTN e1003126 10.1371/journal.pgen.1003126.
45. Mortier-Barrière, I., Velten, M., Dupaigne, P., Mirouze, N., Piétrement, O., McGovern, S., Fichant, G., Martin, B., Noirot, P., Le Cam, E., et al. (2007). A key presynaptic role in transformation for a widespread bacterial protein:: DprA conveys incoming ssDNA to RecA. Cell *130*, 824-836. 10.1016/j.cell.2007.07.038.
46. Azeroglu, B., and Leach, D.R.F. (2017). RecG controls DNA amplification at double-strand breaks and arrested replication forks. FEBS Lett *591*, 1101-1113. 10.1002/1873-3468.12583.
47. Azeroglu, B., Mawer, J.S., Cockram, C.A., White, M.A., Hasan, A.M., Filatenkova, M., and Leach, D.R. (2016). RecG Directs DNA Synthesis during Double-Strand Break Repair. PLoS Genet *12*, e1005799. 10.1371/journal.pgen.1005799.
48. Symington, L.S. (2014). End resection at double-strand breaks: mechanism and regulation. Cold Spring Harb Perspect Biol *6*. 10.1101/cshperspect.a016436.
49. Yeeles, J.T., and Dillingham, M.S. (2007). A dual-nuclease mechanism for DNA break processing by AddAB-type helicase-nucleases. J Mol Biol *371*, 66-78. 10.1016/j.jmb.2007.05.053.
50. Cox, M.M., Goodman, M.F., Keck, J.L., van Oijen, A., Lovett, S.T., and Robinson, A. (2023). Generation and Repair of Postreplication Gaps in Escherichia coli. Microbiol Mol Biol Rev *87*, e0007822. 10.1128/mmbr.00078-22.
51. Nirwal, S., Czarnocki-Cieciura, M., Chaudhary, A., Zajko, W., Skowronek, K., Chamera, S., Figiel, M., and Nowotny, M. (2023). Mechanism of RecF-RecO-RecR cooperation in bacterial homologous recombination. Nat Struct Mol Biol *30*, 650-660. 10.1038/s41594-023-00967-z.
52. Bell, J.C., and Kowalczykowski, S.C. (2016). RecA: Regulation and Mechanism of a Molecular Search Engine: (Trends in Biochemical Sciences, June 2016, Vol. 41, No. 6, 491--507). Trends Biochem Sci *41*, 646. 10.1016/j.tibs.2016.05.006.

53. Lin, Z.G., Kong, H.Z., Nei, M., and Ma, H. (2006). Origins and evolution of the gene family:: Evidence for ancient gene duplication and endosymbiotic gene transfer. P Natl Acad Sci USA *103*, 10328-10333. 10.1073/pnas.0604232103.
54. West, S.C. (1997). Processing of recombination intermediates by the RuvABC proteins. Annu Rev Genet *31*, 213-244. 10.1146/annurev.genet.31.1.213.
55. Bianco, P.R. (2015). I came to a fork in the DNA and there was RecG. Prog Biophys Mol Biol *117*, 166-173. 10.1016/j.pbiomolbio.2015.01.001.
56. Lloyd, R.G., and Rudolph, C.J. (2016). 25 years on and no end in sight: a perspective on the role of RecG protein. Curr Genet *62*, 827-840. 10.1007/s00294-016-0589-z.
57. Shereda, R.D., Kozlov, A.G., Lohman, T.M., Cox, M.M., and Keck, J.L. (2008). SSB as an organizer/mobilizer of genome maintenance complexes. Crit Rev Biochem Mol Biol *43*, 289-318. 10.1080/10409230802341296.
58. Lecointe, F., Serena, C., Velten, M., Costes, A., McGovern, S., Meile, J.C., Errington, J., Ehrlich, S.D., Noirot, P., and Polard, P. (2007). Anticipating chromosomal replication fork arrest: SSB targets repair DNA helicases to active forks. EMBO J *26*, 4239-4251. 10.1038/sj.emboj.7601848.
59. Carrasco, B., Torres, R., Moreno-Del Alamo, M., Ramos, C., Ayora, S., and Alonso, J.C. (2024). Processing of stalled replication forks in Bacillus subtilis. FEMS Microbiol Rev *48*. 10.1093/femsre/fuad065.
60. Sanchez, H., Carrasco, B., Cozar, M.C., and Alonso, J.C. (2007). Bacillus subtilis RecG branch migration translocase is required for DNA repair and chromosomal segregation. Mol Microbiol *65*, 920-935. 10.1111/j.1365-2958.2007.05835.x.
61. Torres, R., Gandara, C., Carrasco, B., Baquedano, I., Ayora, S., and Alonso, J.C. (2021). DisA Limits RecG Activities at Stalled or Reversed Replication Forks. Cells *10*. 10.3390/cells10061357.
62. Torres, R., Romero, H., Rodriguez-Cerrato, V., and Alonso, J.C. (2017). Interplay between Bacillus subtilis RecD2 and the RecG or RuvAB helicase in recombinational repair. DNA Repair (Amst) *55*, 40-46. 10.1016/j.dnarep.2017.05.004.
63. Tanaka, T., and Masai, H. (2006). Stabilization of a stalled replication fork by concerted actions of two helicases. J Biol Chem *281*, 3484-3493. 10.1074/jbc.M510979200.
64. McGlynn, P., Al-Deib, A.A., Liu, J., Marians, K.J., and Lloyd, R.G. (1997). The DNA replication protein PriA and the recombination protein RecG bind D-loops. J Mol Biol *270*, 212-221. 10.1006/jmbi.1997.1120.
65. Sun, B., Pandey, M., Inman, J.T., Yang, Y., Kashlev, M., Patel, S.S., and Wang, M.D. (2015). T7 replisome directly overcomes DNA damage. Nat Commun *6*, 10260. 10.1038/ncomms10260.
66. Fernandez, S., Ayora, S., and Alonso, J.C. (2000). Bacillus subtilis homologous recombination: genes and products. Res Microbiol *151*, 481-486. 10.1016/s0923-2508(00)00165-0.
67. Unciuleac, M.C., and Shuman, S. (2010). Double strand break unwinding and resection by the mycobacterial helicase-nuclease AdnAB in the presence of single strand DNA-binding protein (SSB). J Biol Chem *285*, 34319-34329. 10.1074/jbc.M110.162925.
68. Gupta, R., Unciuleac, M.C., Shuman, S., and Glickman, M.S. (2017). Homologous recombination mediated by the mycobacterial AdnAB helicase without end resection by the AdnAB nucleases. Nucleic Acids Res *45*, 762-774. 10.1093/nar/gkw1130.
69. Su'etsugu, M., and Errington, J. (2011). The replicase sliding clamp dynamically accumulates behind progressing replication forks in *Bacillus subtilis* cells. Mol Cell *41*, 720-732. 10.1016/j.molcel.2011.02.024.
70. Reyes-Lamothe, R., Sherratt, D.J., and Leake, M.C. (2010). Stoichiometry and architecture of active DNA replication machinery in Escherichia coli. Science *328*, 498-501. 10.1126/science.1185757.

71. Yeeles, J.T., van Aelst, K., Dillingham, M.S., and Moreno-Herrero, F. (2011). Recombination hotspots and single-stranded DNA binding proteins couple DNA translocation to DNA unwinding by the AddAB helicase-nuclease. Mol Cell *42*, 806-816. 10.1016/j.molcel.2011.04.012.
72. Umezu, K., and Kolodner, R.D. (1994). Protein interactions in genetic recombination in Escherichia coli. Interactions involving RecO and RecR overcome the inhibition of RecA by single-stranded DNA-binding protein. J Biol Chem *269*, 30005-30013.
73. Hobbs, M.D., Sakai, A., and Cox, M.M. (2007). SSB protein limits RecOR binding onto single-stranded DNA. J Biol Chem *282*, 11058-11067. 10.1074/jbc.M611007200.
74. Inoue, J., Honda, M., Ikawa, S., Shibata, T., and Mikawa, T. (2008). The process of displacing the single-stranded DNA-binding protein from single-stranded DNA by RecO and RecR proteins. Nucleic Acids Res *36*, 94-109. 10.1093/nar/gkm1004.
75. Manfredi, C., Carrasco, B., Ayora, S., and Alonso, J.C. (2008). Bacillus subtilis RecO nucleates RecA onto SsbA-coated single-stranded DNA. J Biol Chem *283*, 24837-24847. 10.1074/jbc.M802002200.
76. Bonde, N.J., Henry, C., Wood, E.A., Cox, M.M., and Keck, J.L. (2023). Interaction with the carboxy-terminal tip of SSB is critical for RecG function in E. coli. Nucleic Acids Res *51*, 3735-3753. 10.1093/nar/gkad162.
77. Buss, J.A., Kimura, Y., and Bianco, P.R. (2008). RecG interacts directly with SSB: implications for stalled replication fork regression. Nucleic Acids Research *36*, 7029-7042. 10.1093/nar/gkn795.
78. Kozlov, A.G., Jezewska, M.J., Bujalowski, W., and Lohman, T.M. (2010). Binding Specificity of Single-Stranded DNA Binding Protein for the χ Subunit of DNA pol III Holoenzyme and PriA Helicase. Biochemistry-Us *49*, 3555-3566. 10.1021/bi100069s.
79. Morimatsu, K., and Kowalczykowski, S.C. (2003). RecFOR proteins load RecA protein onto gapped DNA to accelerate DNA strand exchange: a universal step of recombinational repair. Mol Cell *11*, 1337-1347. 10.1016/s1097-2765(03)00188-6.
80. Lenhart, J.S., Brandes, E.R., Schroeder, J.W., Sorenson, R.J., Showalter, H.D., and Simmons, L.A. (2014). RecO and RecR are necessary for RecA loading in response to DNA damage and replication fork stress. J Bacteriol *196*, 2851-2860. 10.1128/JB.01494-14.
81. Henry, C., Mbele, N., and Cox, M.M. (2023). RecF protein targeting to postreplication (daughter strand) gaps I: DNA binding by RecF and RecFR. Nucleic Acids Res *51*, 5699-5713. 10.1093/nar/gkad311.
82. Henry, C., Kaur, G., Cherry, M.E., Henrikus, S.S., Bonde, N.J., Sharma, N., Beyer, H.A., Wood, E.A., Chitteni-Pattu, S., van Oijen, A.M., et al. (2023). RecF protein targeting to post-replication (daughter strand) gaps II: RecF interaction with replisomes. Nucleic Acids Res *51*, 5714-5742. 10.1093/nar/gkad310.
83. Smith, G.R. (2012). How RecBCD enzyme and Chi promote DNA break repair and recombination: a molecular biologist's view. Microbiol Mol Biol Rev *76*, 217-228. 10.1128/MMBR.05026-11.
84. Conwell, S., Dahmen, S., Cranford, M., Long, D., Cortez, D., and Dewar, J. (2025). Resolution of collapsed forks is separate from completion of DNA synthesis. Submitted.
85. Ayora, S., Carrasco, B., Doncel-Perez, E., Lurz, R., and Alonso, J.C. (2004). Bacillus subtilis RecU protein cleaves Holliday junctions and anneals single-stranded DNA. Proc Natl Acad Sci U S A *101*, 452-457. 10.1073/pnas.2533829100.
86. Aussel, L., Barre, F.X., Aroyo, M., Stasiak, A., Stasiak, A.Z., and Sherratt, D. (2002). FtsK Is a DNA motor protein that activates chromosome dimer resolution by switching the catalytic state of the XerC and XerD recombinases. Cell *108*, 195-205.
87. Kato, J.-I., Nishimura, Y., Imamura, R., Niki, H., Hiraga, S., and Suzuki, H. (1990). New topoisomerase essential for chromosome segregation in E. coli. Cell *63*, 393-404.

88. Lucet, I., Feucht, A., Yudkin, M.D., and Errington, J. (2000). Direct interaction between the cell division protein FtsZ and the cell differentiation protein SpoIIE. EMBO J. *19*, 1467-1475.
89. Schindelin, J., Arganda-Carreras, I., Frise, E., Kaynig, V., Longair, M., Pietzsch, T., Preibisch, S., Rueden, C., Saalfeld, S., Schmid, B., et al. (2012). Fiji: an open-source platform for biological-image analysis. Nat. Methods *9*, 676-682. 10.1038/nmeth.2019.
90. Untergasser, A., Nijveen, H., Rao, X., Bisseling, T., Geurts, R., and Leunissen, J.A. (2007). Primer3Plus, an enhanced web interface to Primer3. Nucleic Acids Res *35*, W71-74. 10.1093/nar/gkm306.
91. Delano, W.L. (2002). The PyMOL Molecular Graphics System.
92. Hanahan, D., Jessee, J., and Bloom, F.R. (1991). Plasmid transformation of Escherichia coli and other bacteria. Methods Enzymol *204*, 63-113. 10.1016/0076-6879(91)04006-a.
93. Anagnostopoulos, C., and Spizizen, J. (1961). Requirements for transformation in *Bacillus subtilis*. J. Bacteriol. *81*, 741-746.
94. Abramson, J., Adler, J., Dunger, J., Evans, R., Green, T., Pritzel, A., Ronneberger, O., Willmore, L., Ballard, A.J., Bambrick, J., et al. (2024). Accurate structure prediction of biomolecular interactions with AlphaFold 3. Nature *630*, 493-500. 10.1038/s41586-024-07487-w.
95. Krajewski, W.W., Fu, X., Wilkinson, M., Cronin, N.B., Dillingham, M.S., and Wigley, D.B. (2014). Structural basis for translocation by AddAB helicase-nuclease and its arrest at chi sites. Nature *508*, 416-419. 10.1038/nature13037.

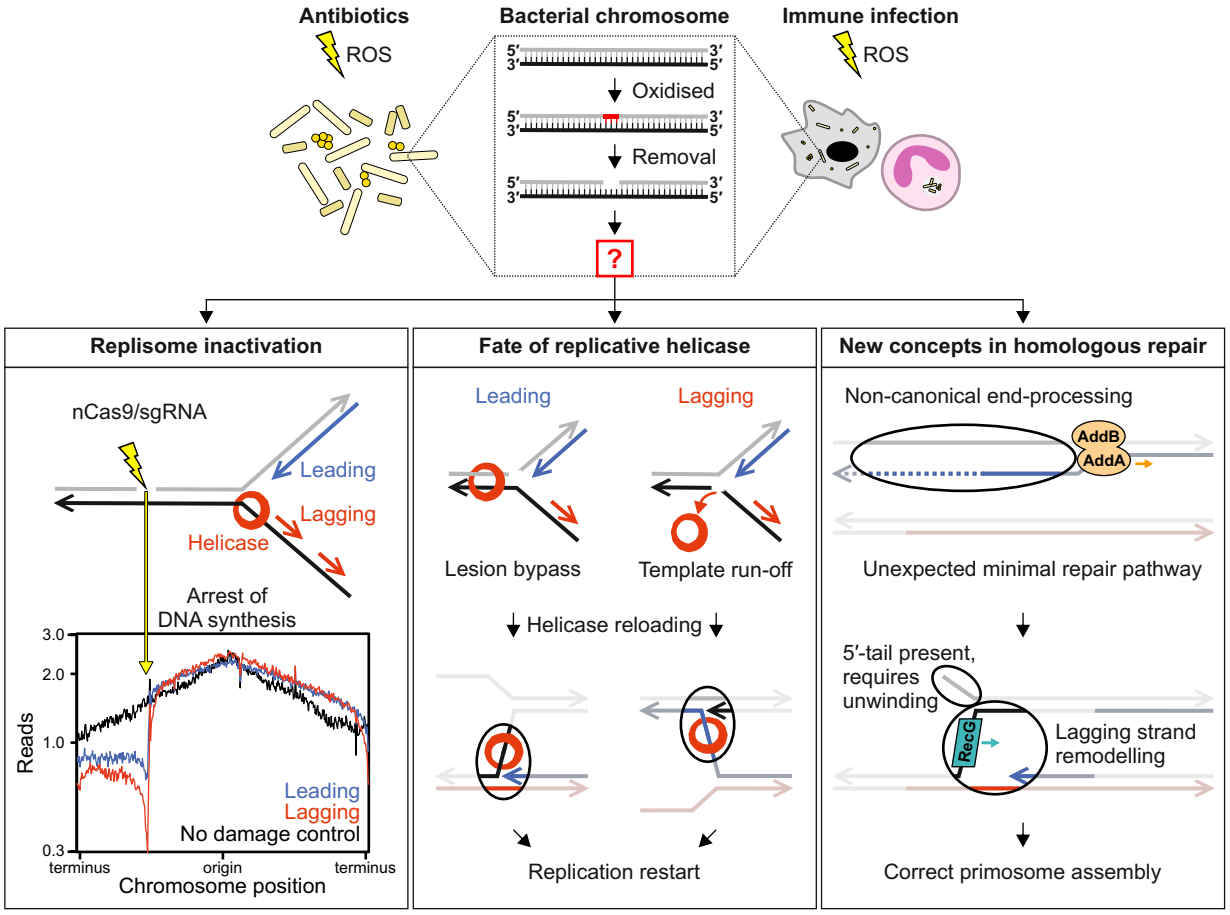

GRAPHICAL ABSTRACT

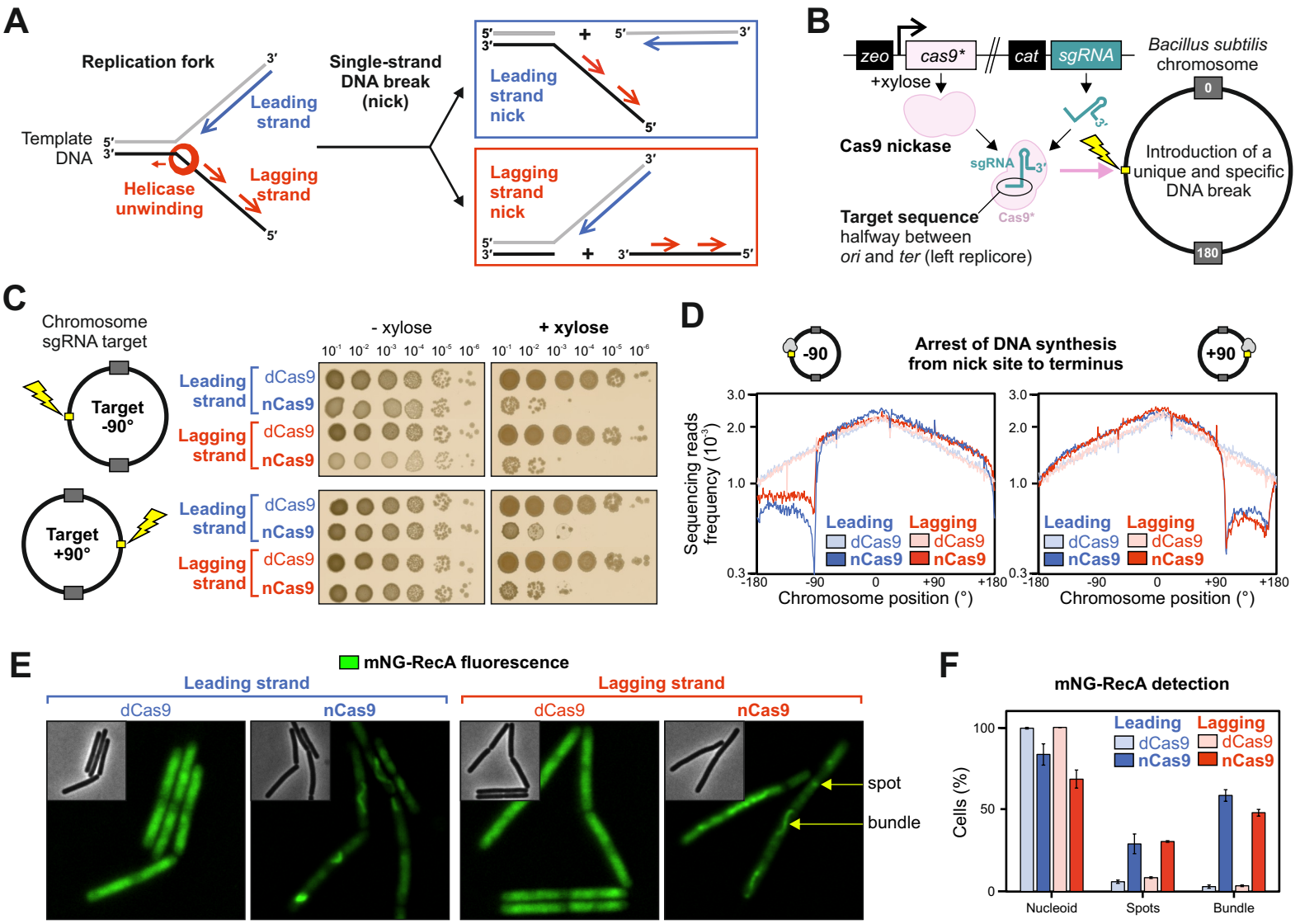
A
Replication fork
Template DNA
Leading strand
Lagging strand
Helicase unwinding
Single-strand DNA break (nick)
Leading strand nick
Lagging strand nick
B
zeo
cas9*
cat
sgRNA
+xylose
Bacillus subtilis chromosome
Cas9 nickase
sgRNA
Cas9*
Target sequence halfway between ori and ter (left replicore)
Introduction of a unique and specific DNA break
0
180
C
Chromosome sgRNA target
Target -90°
Target +90°
- xylose
+ xylose
Leading strand
Lagging strand
dCas9
nCas9
D
-90
+90
Arrest of DNA synthesis from nick site to terminus
Sequencing reads frequency (10^-3)
Leading
Lagging
dCas9
nCas9
Chromosome position (°)
E
mNG-RecA fluorescence
Leading strand
Lagging strand
dCas9
nCas9
spot
bundle
F
mNG-RecA detection
Cells (%)
Nucleoid
Spots
Bundle

FIGURE 1

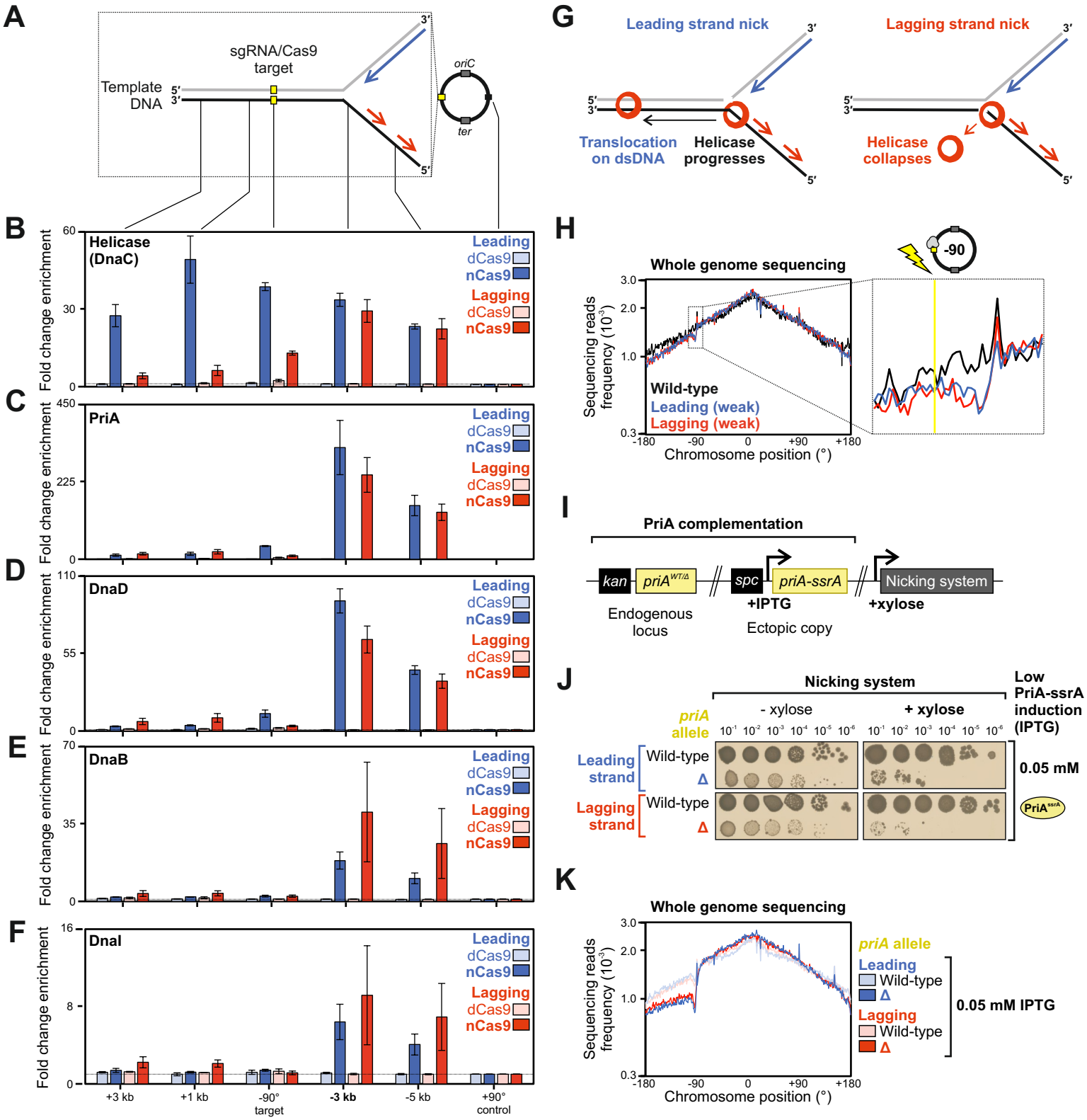
A
sgRNA/Cas9 target
Template DNA
5′
3′
oriC
ter
B
Helicase (DnaC)
Fold change enrichment
Leading
dCas9
nCas9
Lagging
dCas9
nCas9
C
PriA
D
DnaD
E
DnaB
F
DnaI
+3 kb
+1 kb
-90° target
-3 kb
-5 kb
+90° control
G
Leading strand nick
Lagging strand nick
Translocation on dsDNA
Helicase progresses
Helicase collapses
H
Whole genome sequencing
Sequencing reads frequency (10⁻³)
Wild-type
Leading (weak)
Lagging (weak)
Chromosome position (°)
-90
I
PriA complementation
kan
priA WT/Δ
spc
priA-ssrA
Nicking system
Endogenous locus
+IPTG
Ectopic copy
+xylose
J
Nicking system
- xylose
+ xylose
Low PriA-ssrA induction (IPTG)
priA allele
Leading strand
Lagging strand
Wild-type
Δ
0.05 mM
PriA ssrA
K
Whole genome sequencing
priA allele
Leading
Lagging
0.05 mM IPTG

FIGURE 2

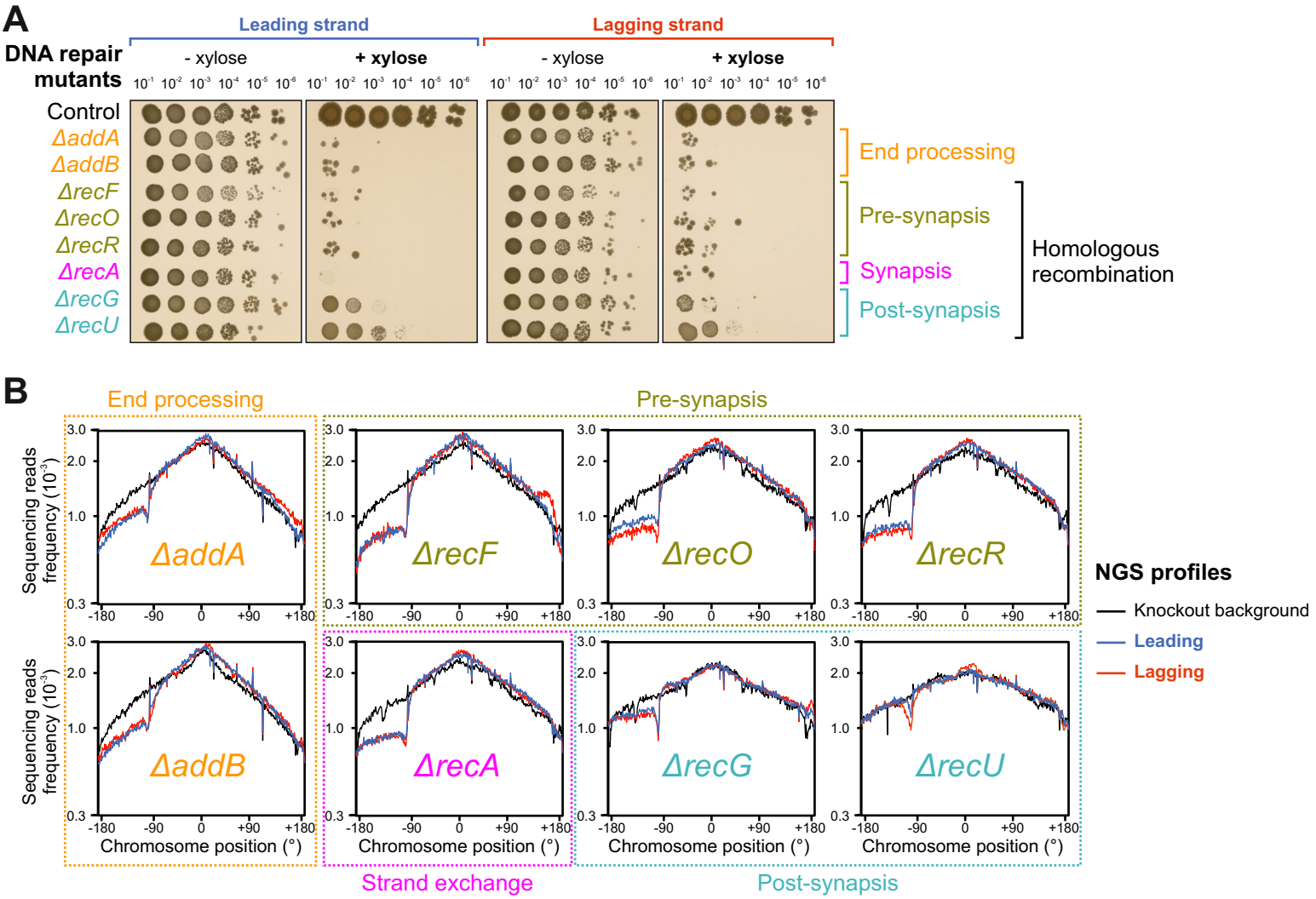
A
DNA repair mutants
Leading strand
Lagging strand
- xylose
+ xylose
- xylose
+ xylose
Control
ΔaddA
ΔaddB
ΔrecF
ΔrecO
ΔrecR
ΔrecA
ΔrecG
ΔrecU
End processing
Pre-synapsis
Synapsis
Post-synapsis
Homologous recombination
B
End processing
Pre-synapsis
Strand exchange
Post-synapsis
Sequencing reads frequency (10⁻³)
Chromosome position (°)
NGS profiles
Knockout background
Leading
Lagging

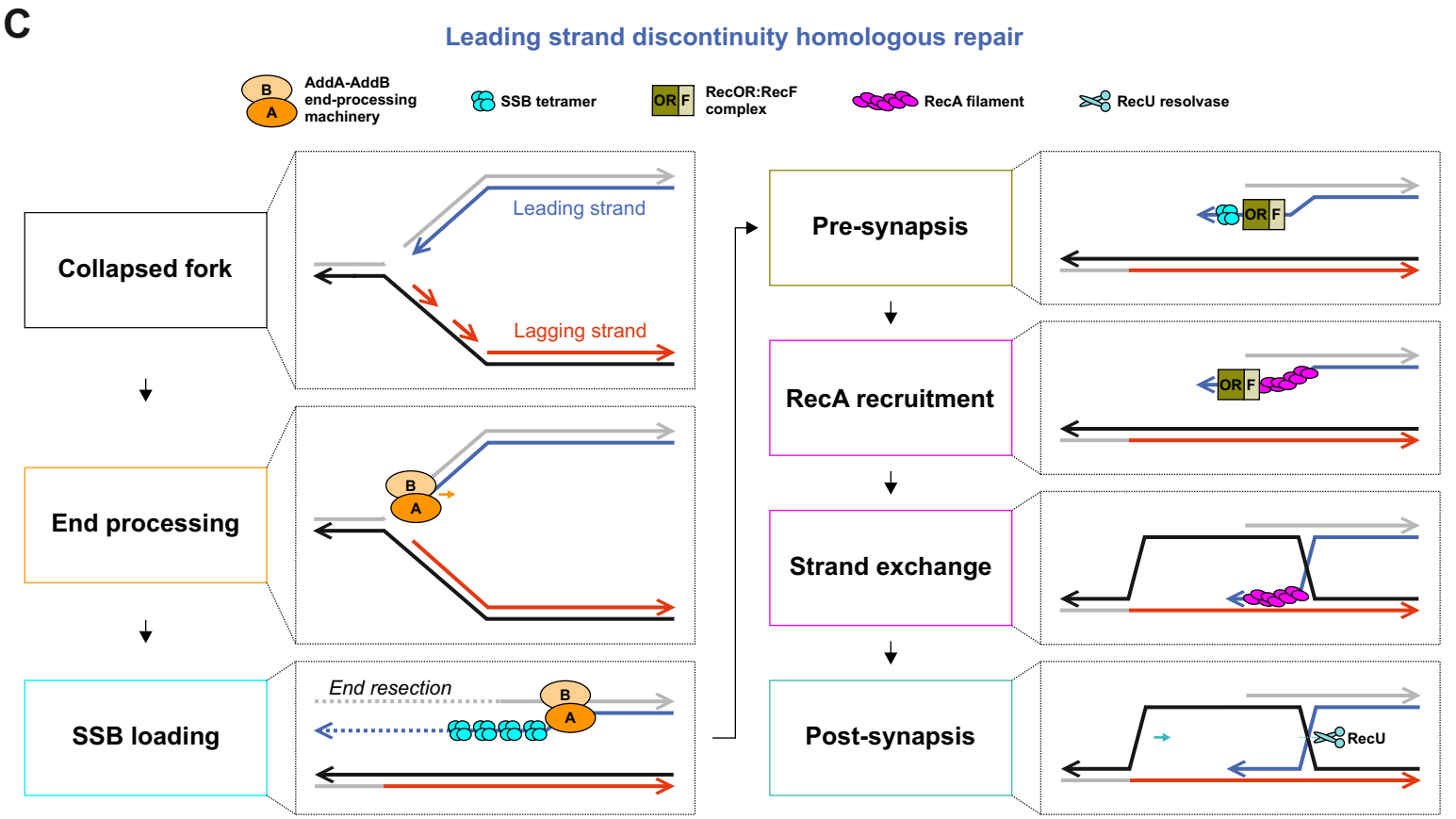
C
Leading strand discontinuity homologous repair
AddA-AddB end-processing machinery
SSB tetramer
RecOR:RecF complex
RecA filament
RecU resolvase
Collapsed fork
Leading strand
Lagging strand
End processing
SSB loading
End resection
Pre-synapsis
RecA recruitment
Strand exchange
Post-synapsis
RecU

FIGURE 3

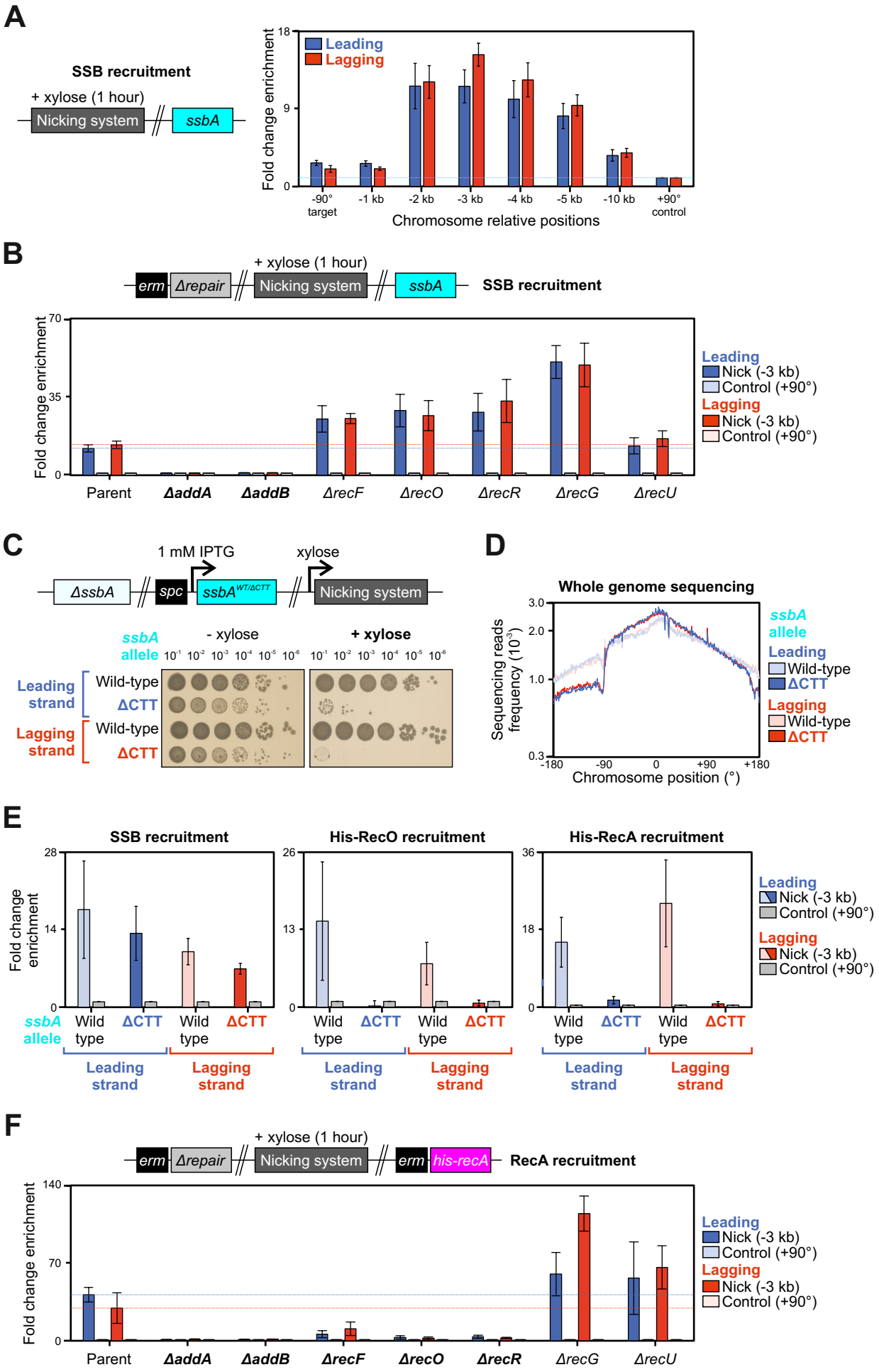
A
SSB recruitment
+ xylose (1 hour)
Nicking system
ssbA
Leading
Lagging
Fold change enrichment
18
9
0
-90° target
-1 kb
-2 kb
-3 kb
-4 kb
-5 kb
-10 kb
+90° control
Chromosome relative positions
B
+ xylose (1 hour)
erm
Δrepair
Nicking system
ssbA
SSB recruitment
Fold change enrichment
70
35
0
Parent
ΔaddA
ΔaddB
ΔrecF
ΔrecO
ΔrecR
ΔrecG
ΔrecU
Leading
Nick (-3 kb)
Control (+90°)
Lagging
Nick (-3 kb)
Control (+90°)
C
1 mM IPTG
xylose
ΔssbA
spc
ssbA WT/ΔCTT
Nicking system
ssbA allele
- xylose
+ xylose
10-1 10-2 10-3 10-4 10-5 10-6
Leading strand
Wild-type
ΔCTT
Lagging strand
Wild-type
ΔCTT
D
Whole genome sequencing
Sequencing reads frequency (10-3)
3.0
2.0
1.0
0.3
-180
-90
0
+90
+180
Chromosome position (°)
ssbA allele
Leading
Wild-type
ΔCTT
Lagging
Wild-type
ΔCTT
E
SSB recruitment
His-RecO recruitment
His-RecA recruitment
Fold change enrichment
28
14
0
26
13
0
36
18
0
ssbA allele
Wild type
ΔCTT
Wild type
ΔCTT
Leading strand
Lagging strand
Leading
Nick (-3 kb)
Control (+90°)
Lagging
Nick (-3 kb)
Control (+90°)
F
+ xylose (1 hour)
erm
Δrepair
Nicking system
erm
his-recA
RecA recruitment
Fold change enrichment
140
70
0
Parent
ΔaddA
ΔaddB
ΔrecF
ΔrecO
ΔrecR
ΔrecG
ΔrecU
Leading
Nick (-3 kb)
Control (+90°)
Lagging
Nick (-3 kb)
Control (+90°)

FIGURE 4

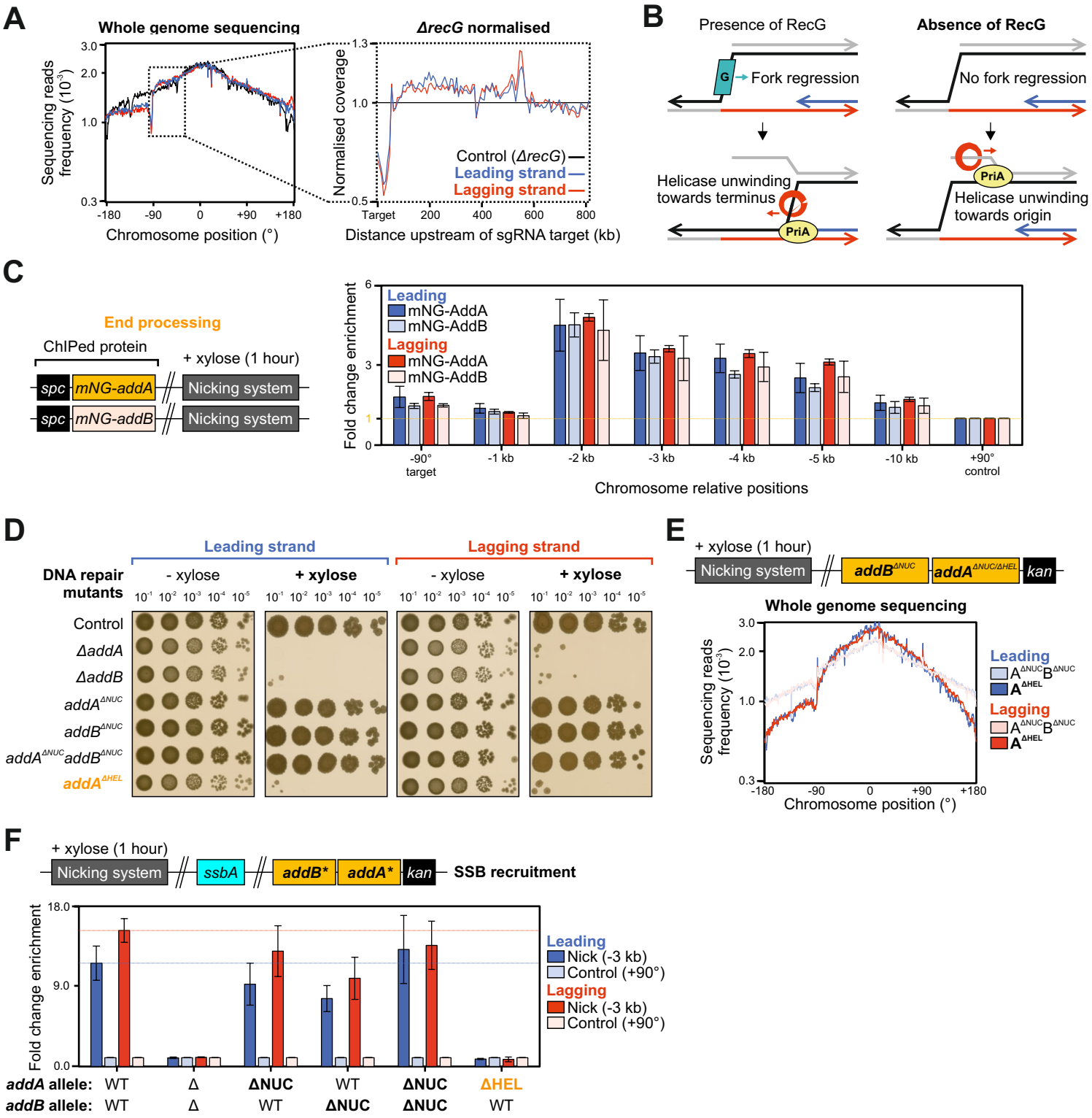
A
Whole genome sequencing
ΔrecG normalised
Sequencing reads frequency (10^-3)
Normalised coverage
Control (ΔrecG)
Leading strand
Lagging strand
Chromosome position (°)
Distance upstream of sgRNA target (kb)
B
Presence of RecG
Absence of RecG
Fork regression
No fork regression
Helicase unwinding towards terminus
Helicase unwinding towards origin
PriA
C
End processing
ChIPed protein
+ xylose (1 hour)
spc
mNG-addA
mNG-addB
Nicking system
Fold change enrichment
Leading
mNG-AddA
mNG-AddB
Lagging
mNG-AddA
mNG-AddB
-90° target
-1 kb
-2 kb
-3 kb
-4 kb
-5 kb
-10 kb
+90° control
Chromosome relative positions
D
Leading strand
Lagging strand
DNA repair mutants
- xylose
+ xylose
Control
ΔaddA
ΔaddB
addA^ΔNUC
addB^ΔNUC
addA^ΔNUC addB^ΔNUC
addA^ΔHEL
E
+ xylose (1 hour)
addB^ΔNUC
addA^ΔNUC/ΔHEL
kan
Whole genome sequencing
Leading
Lagging
F
+ xylose (1 hour)
ssbA
addB*
addA*
kan
SSB recruitment
Fold change enrichment
Leading
Nick (-3 kb)
Control (+90°)
Lagging
Nick (-3 kb)
Control (+90°)
addA allele: WT Δ ΔNUC WT ΔNUC ΔHEL
addB allele: WT Δ WT ΔNUC ΔNUC WT

FIGURE 5

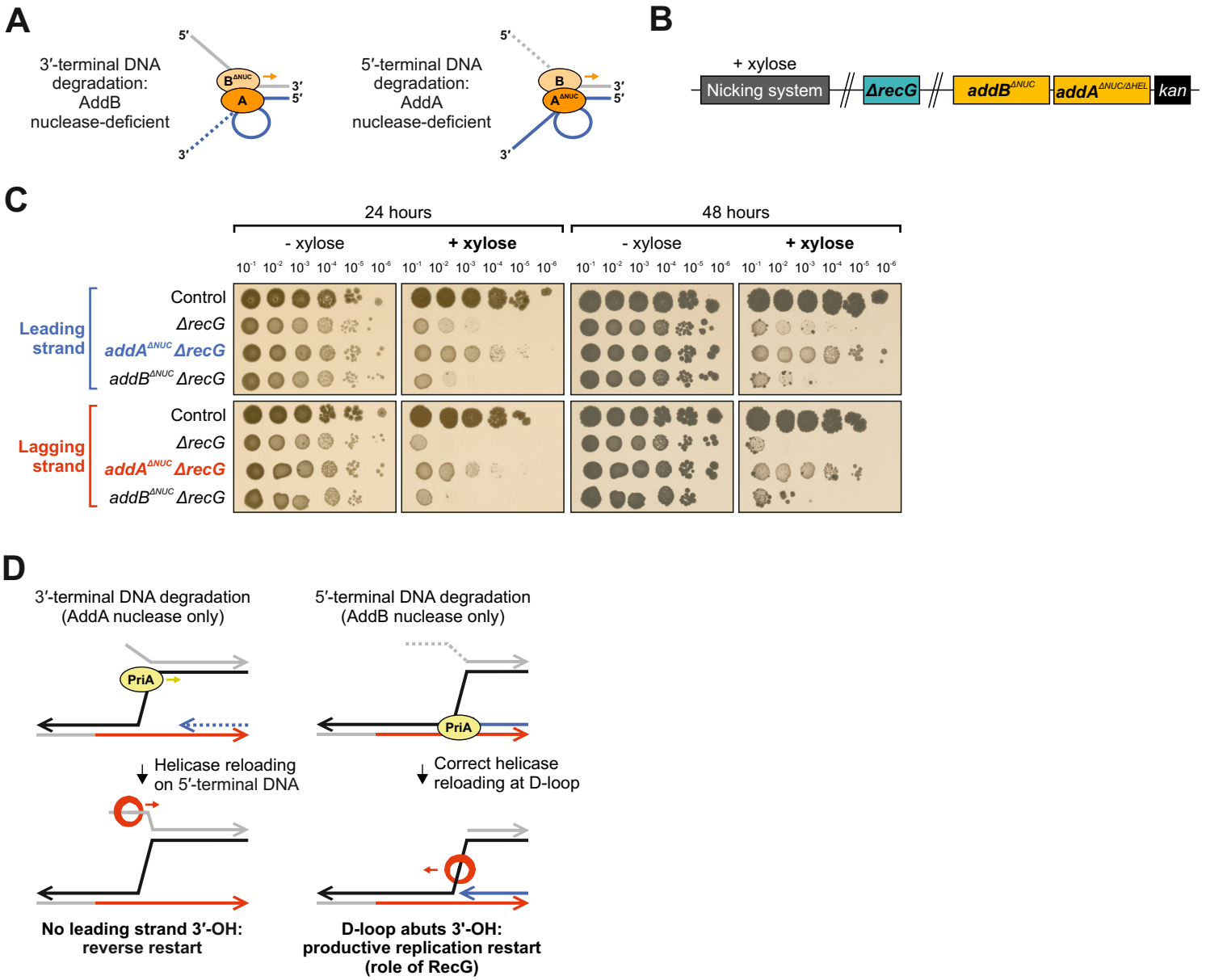
A
3′-terminal DNA degradation: AddB nuclease-deficient
5′-terminal DNA degradation: AddA nuclease-deficient
B
+ xylose
Nicking system
ΔrecG
addB^ΔNUC
addA^ΔNUC/ΔHEL
kan
C
24 hours
48 hours
- xylose
+ xylose
Leading strand
Lagging strand
Control
ΔrecG
addA^ΔNUC ΔrecG
addB^ΔNUC ΔrecG
D
3′-terminal DNA degradation (AddA nuclease only)
5′-terminal DNA degradation (AddB nuclease only)
PriA
Helicase reloading on 5′-terminal DNA
Correct helicase reloading at D-loop
No leading strand 3′-OH: reverse restart
D-loop abuts 3′-OH: productive replication restart (role of RecG)

FIGURE 6

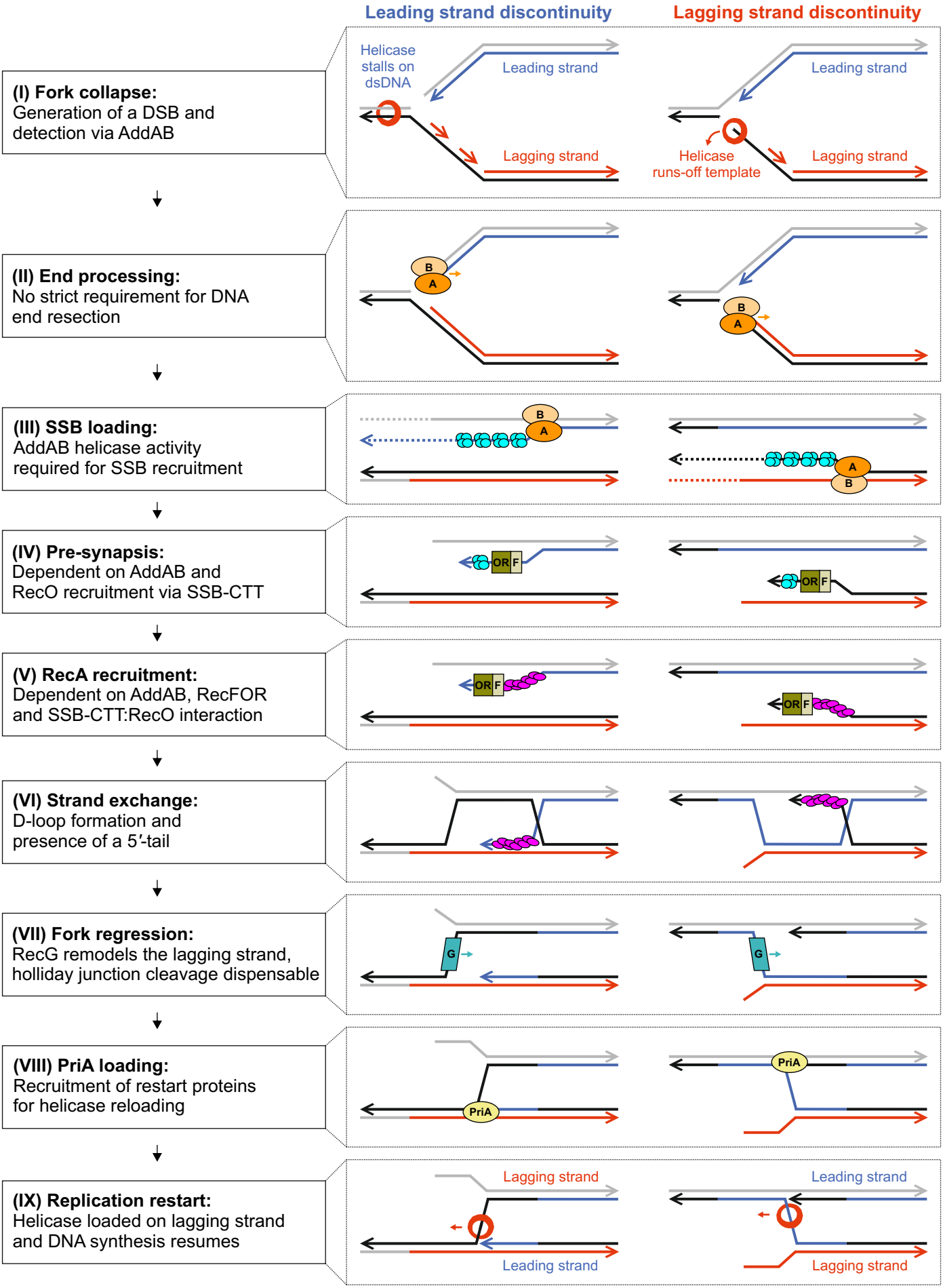
Leading strand discontinuity
Lagging strand discontinuity
(I) Fork collapse:
Generation of a DSB and detection via AddAB
Helicase stalls on dsDNA
Leading strand
Lagging strand
Helicase runs-off template
(II) End processing:
No strict requirement for DNA end resection
B
A
(III) SSB loading:
AddAB helicase activity required for SSB recruitment
(IV) Pre-synapsis:
Dependent on AddAB and RecO recruitment via SSB-CTT
OR F
(V) RecA recruitment:
Dependent on AddAB, RecFOR and SSB-CTT:RecO interaction
(VI) Strand exchange:
D-loop formation and presence of a 5′-tail
(VII) Fork regression:
RecG remodels the lagging strand, holliday junction cleavage dispensable
G
(VIII) PriA loading:
Recruitment of restart proteins for helicase reloading
PriA
(IX) Replication restart:
Helicase loaded on lagging strand and DNA synthesis resumes

FIGURE 7

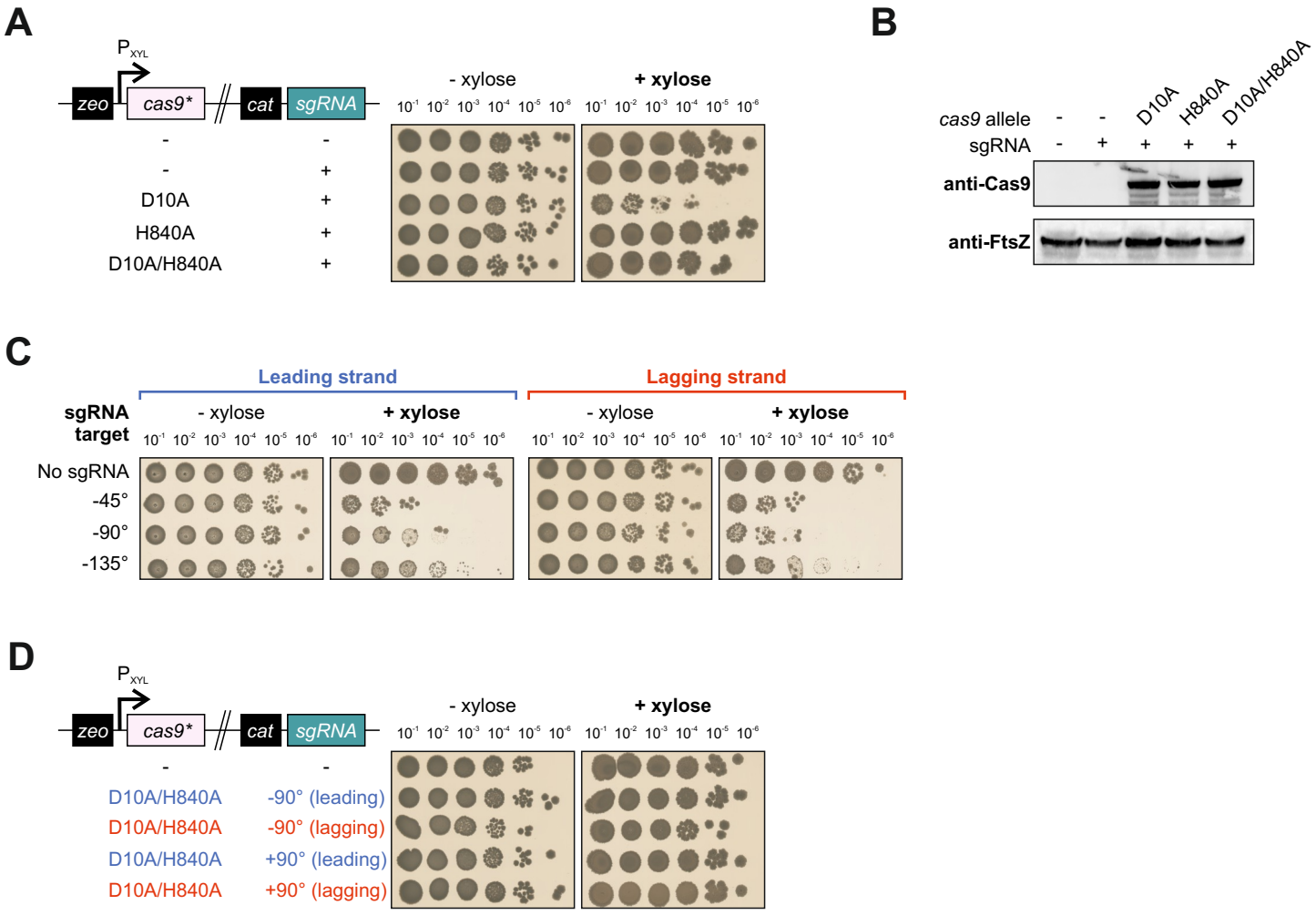

SUPPLEMENTARY FIGURE 1

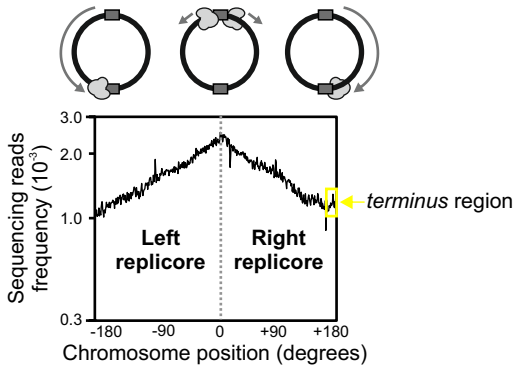

SUPPLEMENTARY FIGURE 2

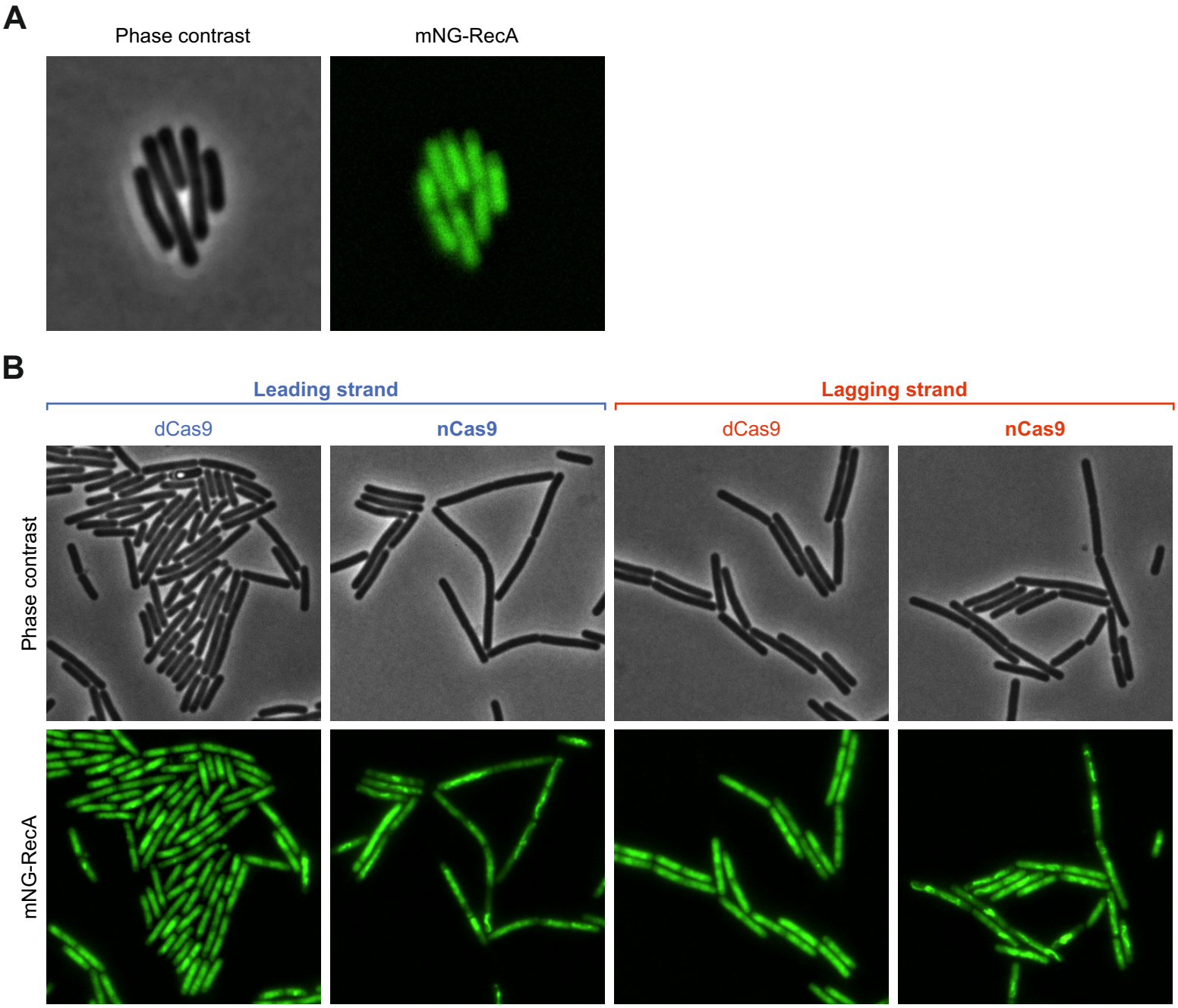

SUPPLEMENTARY FIGURE 3

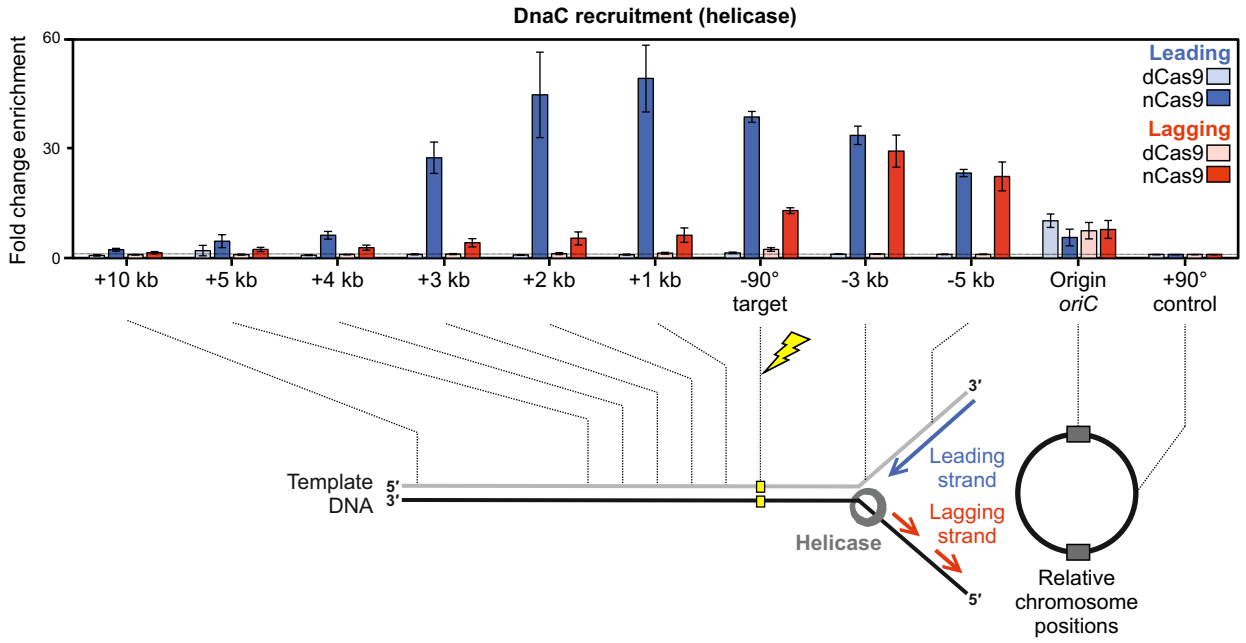

SUPPLEMENTARY FIGURE 4

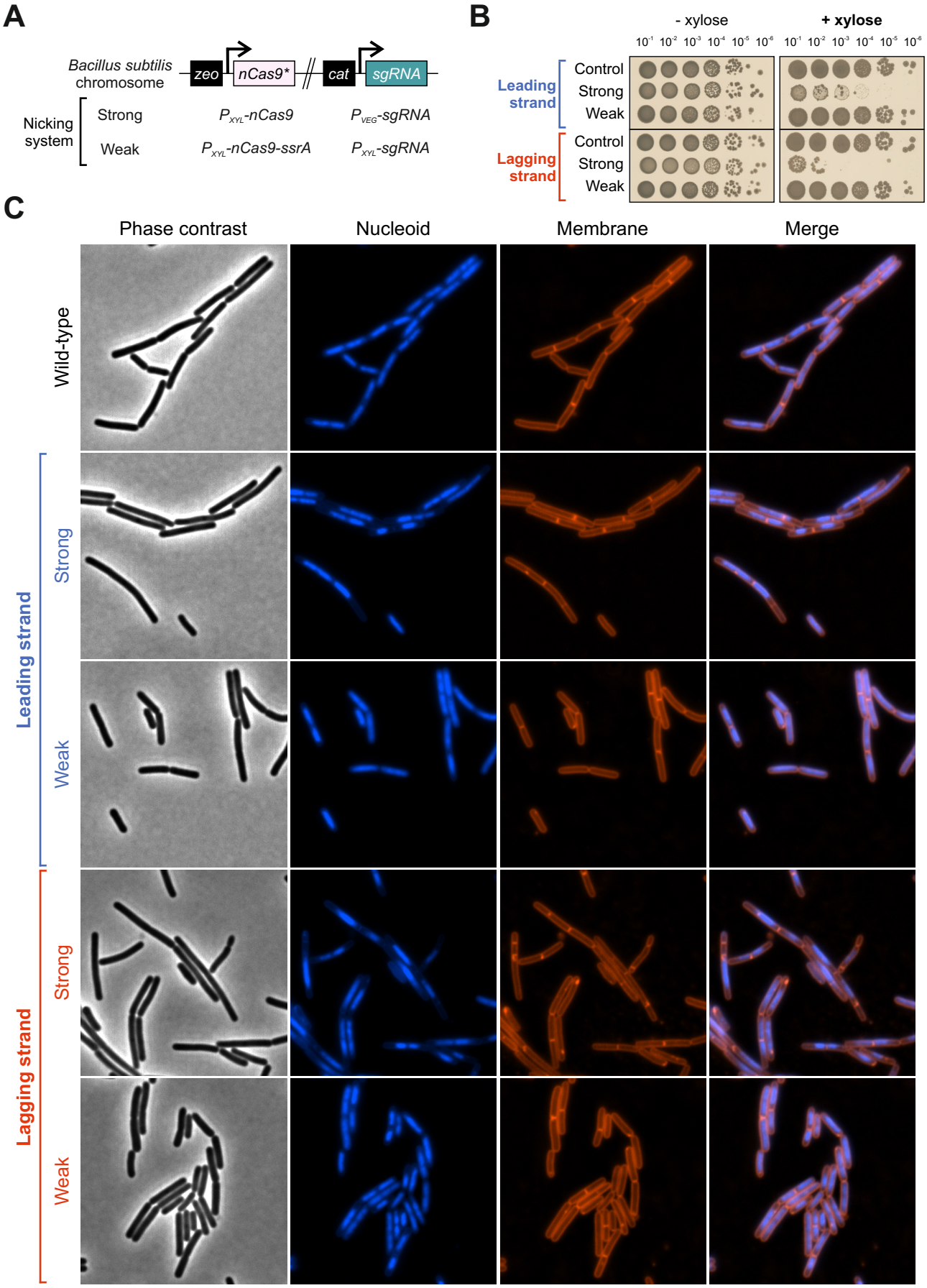

SUPPLEMENTARY FIGURE 5

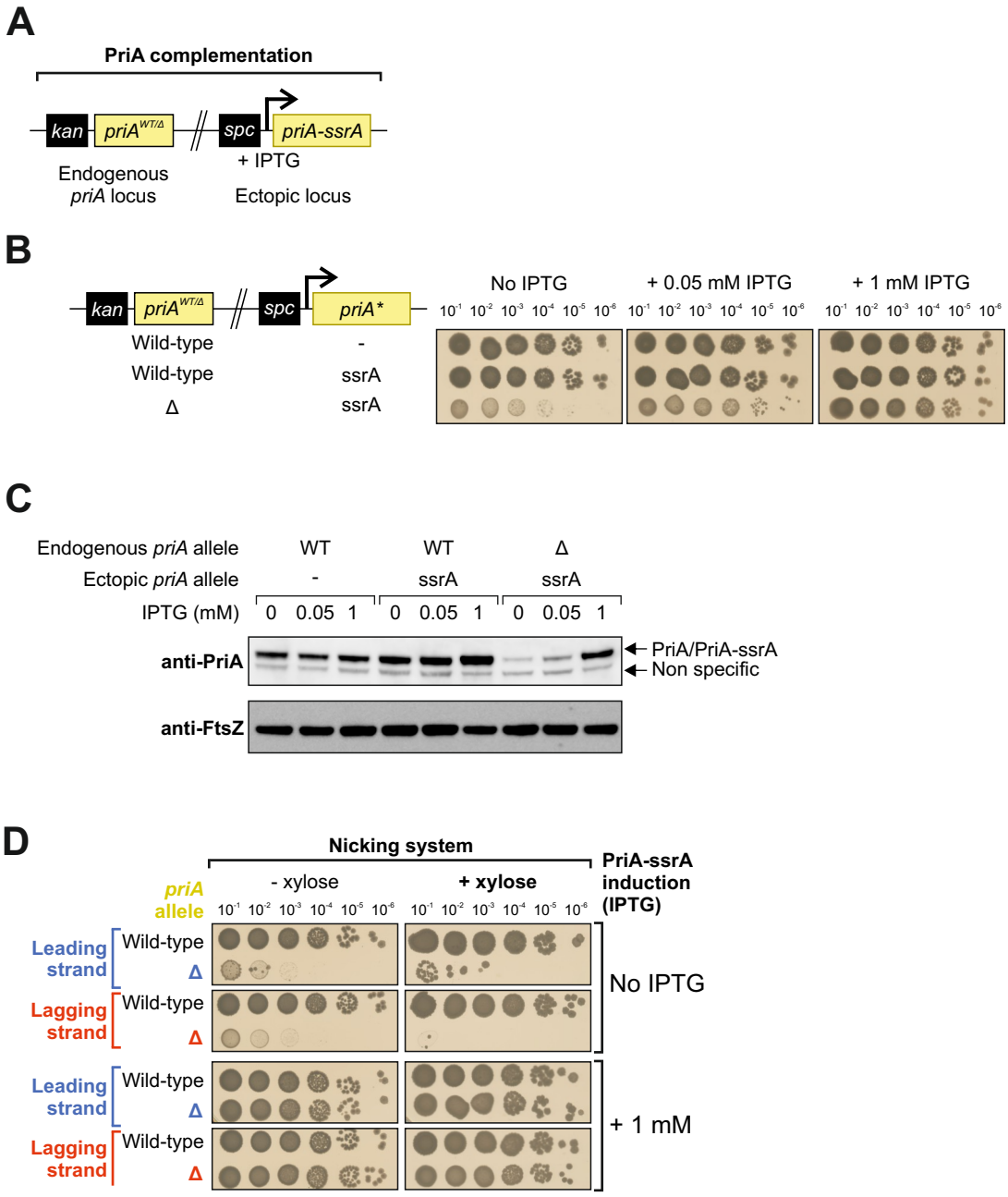

SUPPLEMENTARY FIGURE 6

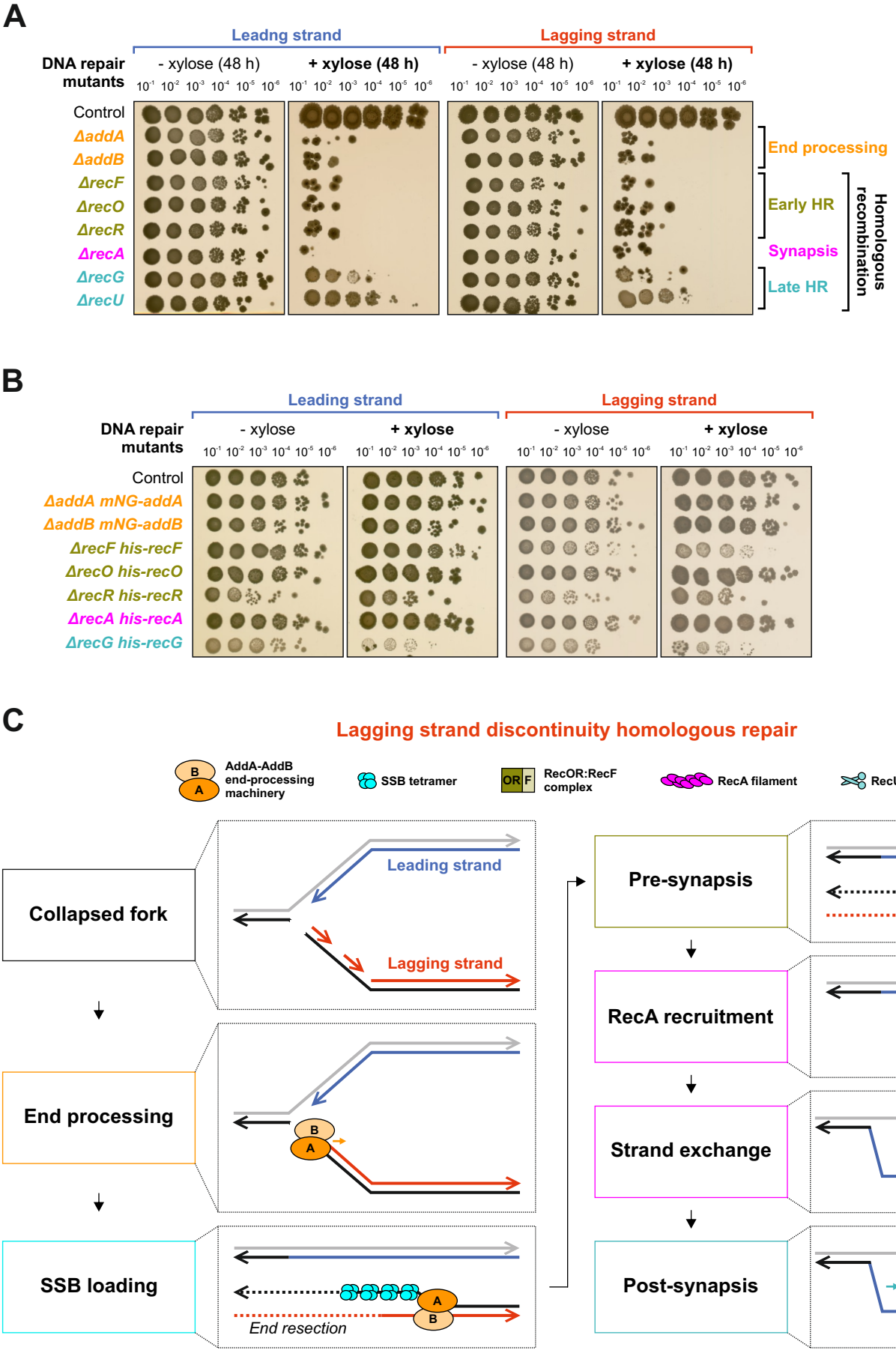

SUPPLEMENTARY FIGURE 7

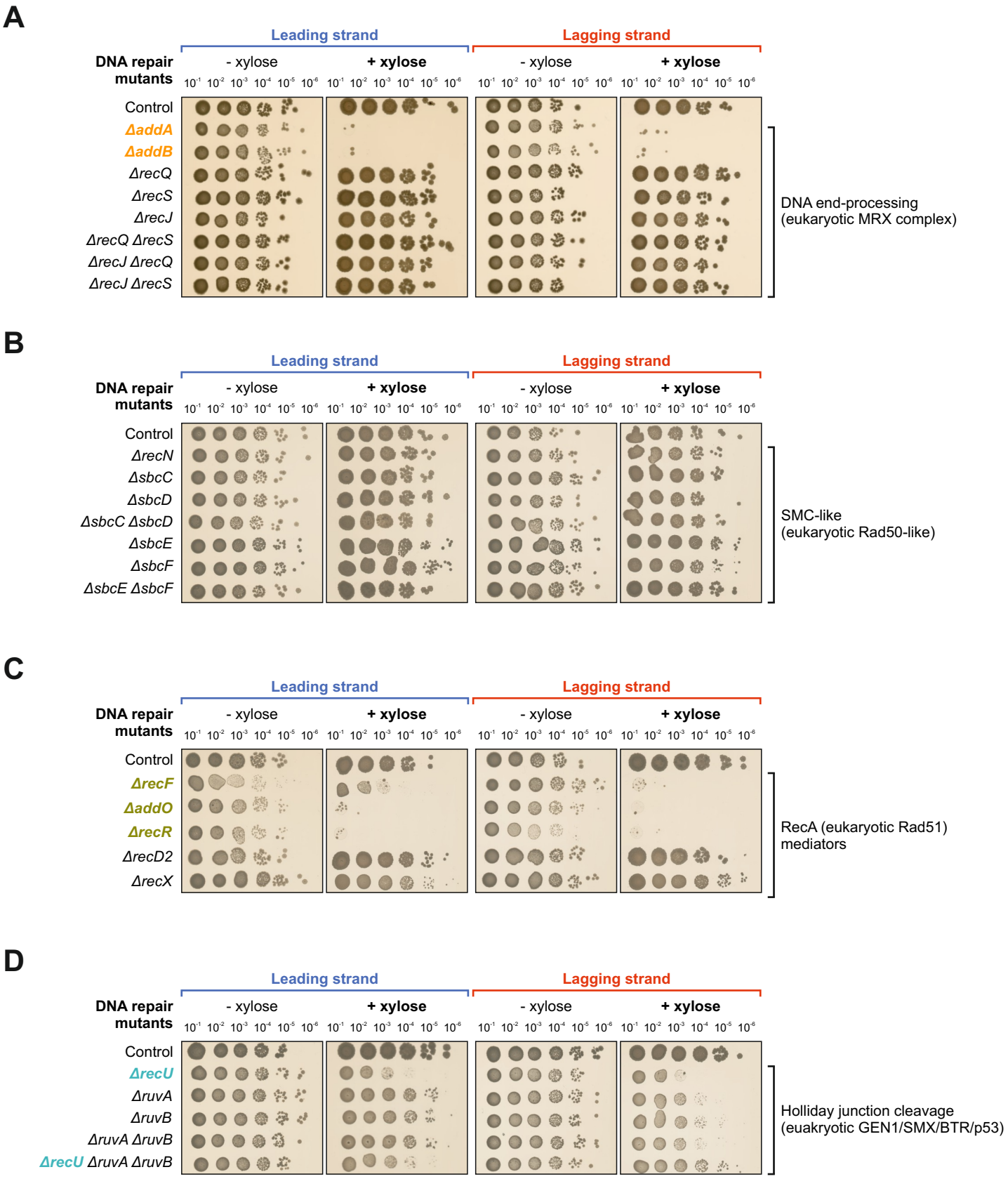

SUPPLEMENTARY FIGURE 8

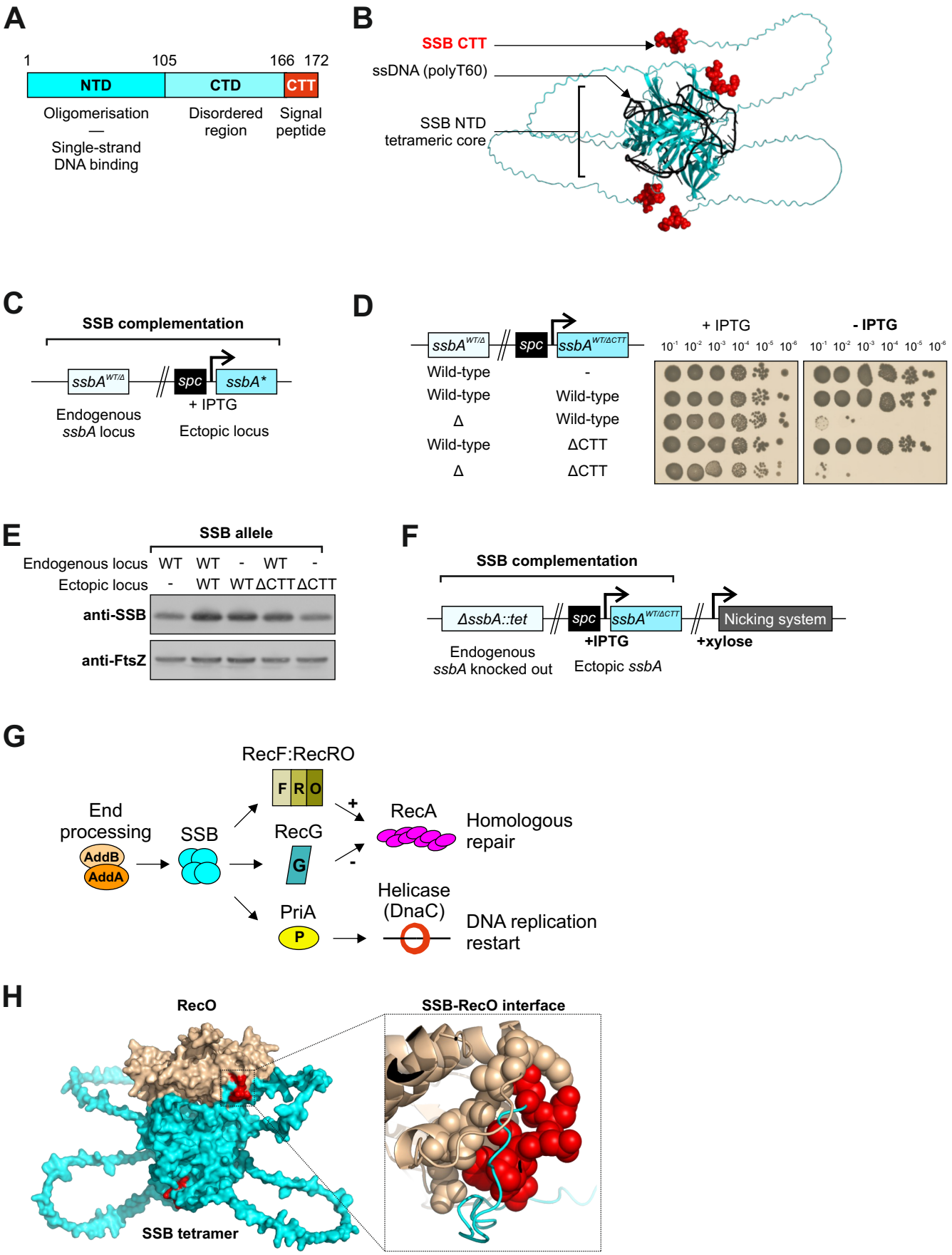

SUPPLEMENTARY FIGURE 9

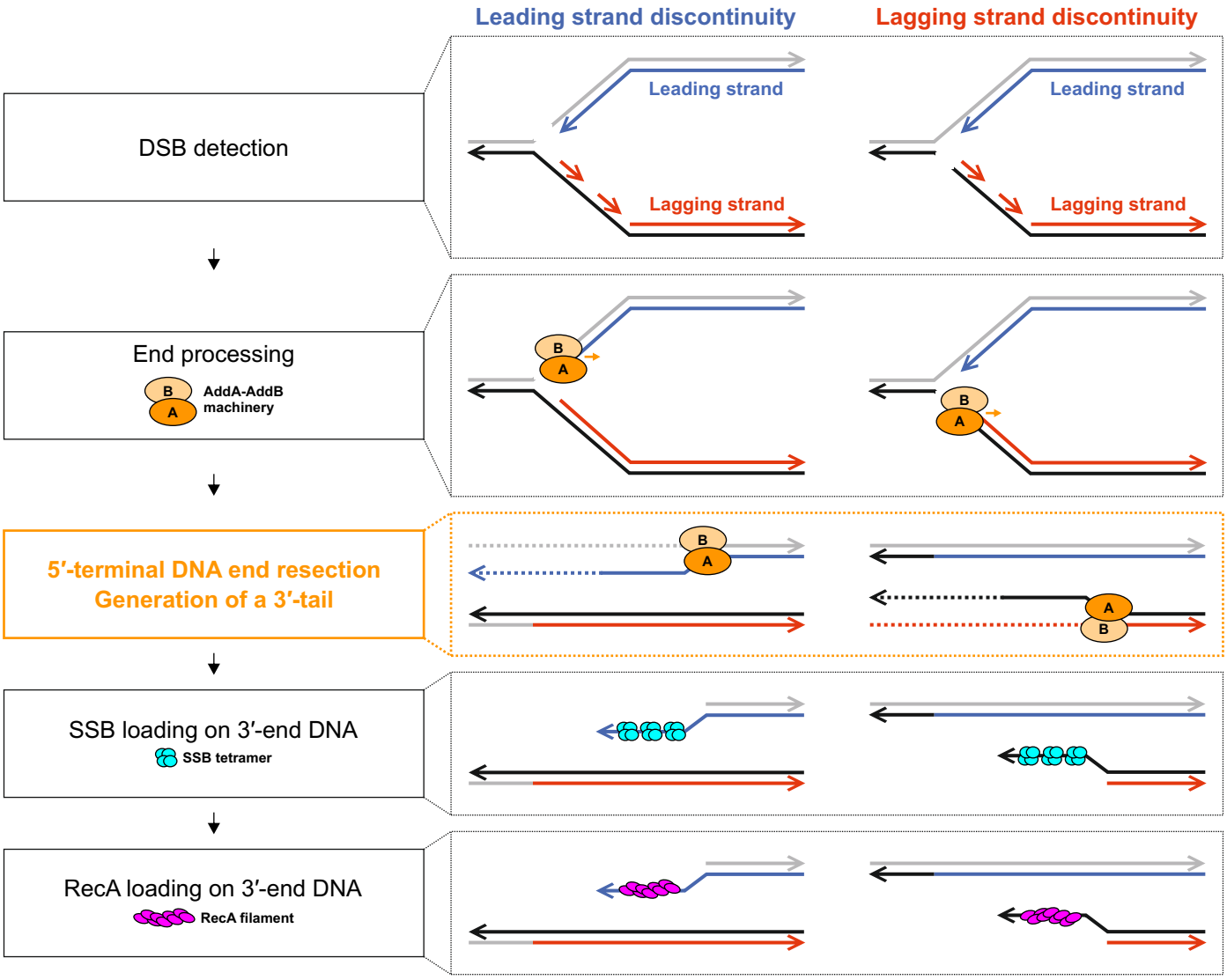

SUPPLEMENTARY FIGURE 10

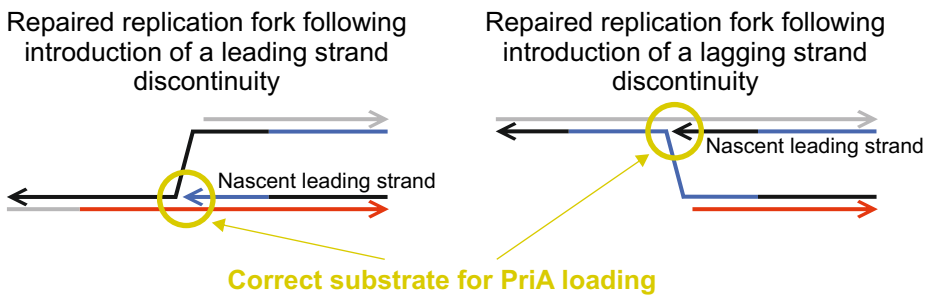

SUPPLEMENTARY FIGURE 11

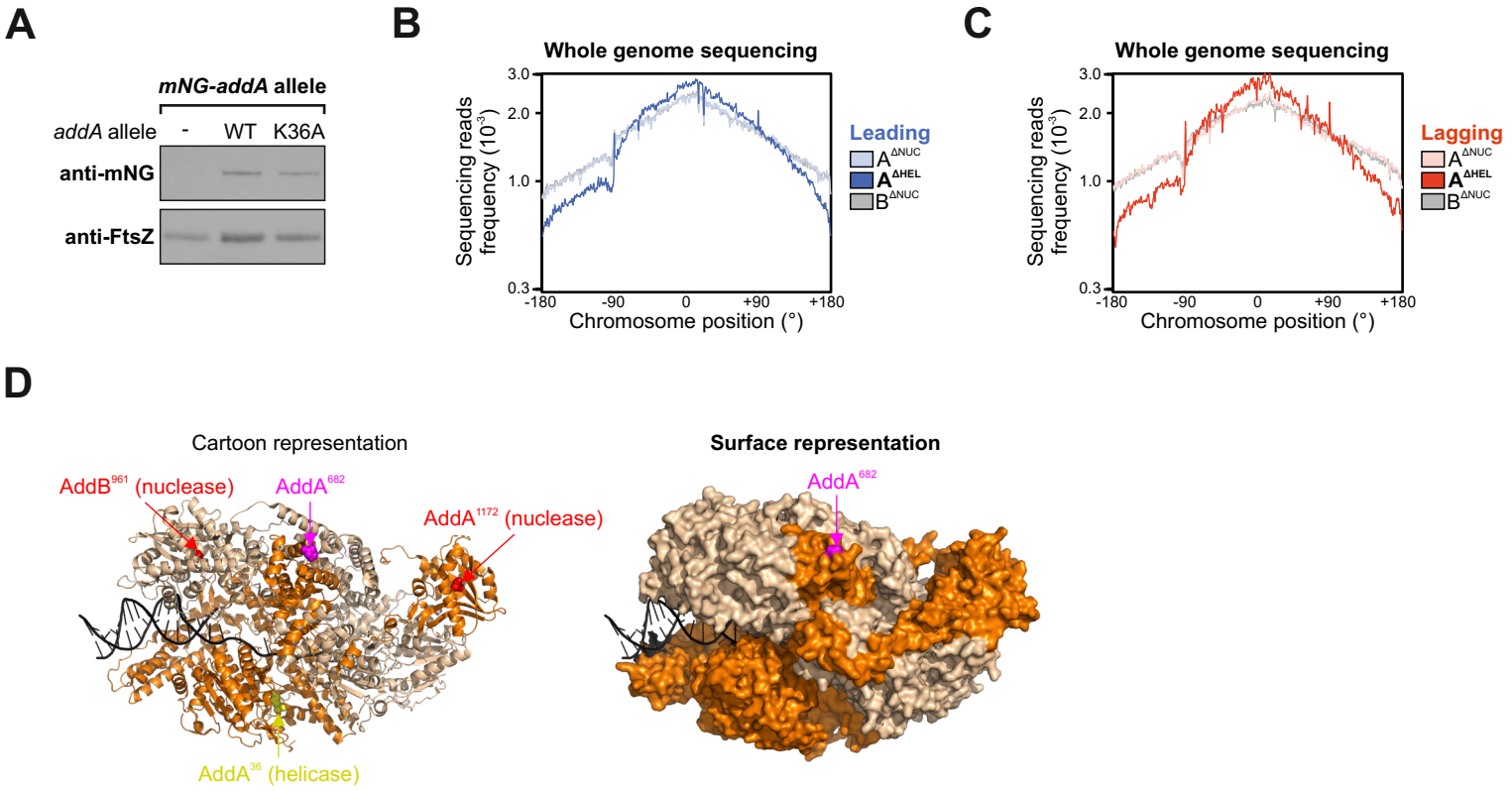

SUPPLEMENTARY FIGURE 12